

Thermodynamics of mantle minerals – I. Physical properties

Lars Stixrude and Carolina Lithgow-Bertelloni

Department of Geological Sciences, University of Michigan, Ann Arbor, MI, USA. E-mail: stixrude@umich.edu

Accepted 2005 March 17. Received 2005 March 16; in original form 2004 October 22

SUMMARY

We present a theory for the computation of phase equilibria and physical properties of multi-component assemblages relevant to the mantle of the Earth. The theory differs from previous treatments in being thermodynamically self-consistent: the theory is based on the concept of fundamental thermodynamic relations appropriately generalized to anisotropic strain and in encompassing elasticity in addition to the usual isotropic thermodynamic properties. In this first paper, we present the development of the theory, discuss its scope, and focus on its application to physical properties of mantle phases at elevated pressure and temperature including the equation of state, thermochemical properties and the elastic wave velocities. We find that the Eulerian finite strain formulation captures the variation of the elastic moduli with compression. The variation of the vibrational frequencies with compression is also cast as a Taylor series expansion in the Eulerian finite strain, the appropriate volume derivative of which leads to an expression for the Grüneisen parameter that agrees well with results from first principles theory. For isotropic materials, the theory contains nine material-specific parameters: the values at ambient conditions of the Helmholtz free energy, volume, bulk and shear moduli, their pressure derivatives, an effective Debye temperature, its first and second logarithmic volume derivatives (γ_0, q_0), and the shear strain derivative of γ . We present and discuss in some detail the results of a global inversion of a wide variety of experimental data and first principles theoretical results, supplemented by systematic relations, for the values of these parameters for 31 mantle species. Among our findings is that the value of q is likely to be significantly greater than unity for most mantle species. We apply the theory to the computation of the shear wave velocity, and temperature and compositional (Fe content) derivatives at relevant mantle pressure temperature conditions. Among the patterns that emerge is that garnet is anomalous in being remarkably insensitive to iron content or temperature as compared with other mantle phases.

Key words: bulk modulus, mantle, shear modulus, thermodynamics.

1 INTRODUCTION

The tools and concepts of thermodynamics are an essential part of any model of planetary evolution, dynamics and structure. The relationship between the internal heat and temperature of a planet as it cools, between temperature and the buoyancy that drives convection, and the extent and consequences of gravitational self-compression are all governed by equilibrium physical properties and understood on the basis of thermodynamics. Thermodynamics is powerful because its scope is so vast; applicable not only to planets but equally to black holes and laboratory samples. This extreme generality also means that the theory must be supplemented with particular knowledge of the materials of interest, values of key physical quantities, and their variations with pressure, temperature and bulk composition.

The materials and conditions of the interior of the Earth present several special challenges. The range of pressure is comparable to the bulk modulus and to the pressure scale of valence band deformation, so that we expect phase transformations and alteration of chemical bonding on very general grounds. At the same time, the range of pressure and temperature is not sufficient to stabilize either of two states that are particularly well understood: the ideal gas and the free electron gas, both of which are important for understanding giant planets and stars. The chemical composition of the terrestrial mantle is also relatively complex with at least five essential oxide components and 10 major solid phases.

Knowledge of the physical properties of mantle minerals provides the essential link between geophysical observations and geodynamics. For example, seismology does not measure energy or temperature; variations in velocity must be related to these geodynamically relevant quantities via experimental measurements. At the same time, many geophysical observations are remarkably precise, placing extreme demands

on the accuracy of any thermodynamic model of the mantle and the experiments or first principles computations that must be used to constrain it.

The multiphase nature of the mantle is central to our understanding of its structure and dynamics. In the transition zone, gravitational self-compression is accommodated mostly by solid–solid phase transformations. Many phase transformations occur over sufficiently narrow intervals of pressure that they are seismically reflective; the comparison of the depth of these reflectors to the pressure of phase transformations gives us one of our most powerful constraints on the composition of the deep interior. Because the pressure at which they occur depends on temperature, phase transformations may also contribute to laterally heterogeneous structure and influence mantle dynamics (Anderson 1987).

Birch (1952) recognized that the unique features of Earth meant that approximate theories, such as the Thomas–Fermi–Dirac model, were not sufficiently accurate or meaningful to teach us about the terrestrial interior. His work emphasized the importance of careful experimental measurements of physical properties at elevated pressure and temperature, a programme that continues with great vigour and that has made great strides since Birch's day in precision and scope. Solid state theory has also undergone major advances over the past several decades, and modern first principles computations have started to play a role in uncovering the physics of mantle phases at high pressure and temperature, and in making quantitative predictions.

The remarkable advances in experimental and theoretical mineral physics have motivated us to an interim synthesis of mantle thermodynamics in the form of a new thermodynamic model and a summary of relevant data. In developing our model, we have borne in mind the need to capture self-consistently and on an equal footing the physical properties of phases, including those that are geodynamically important and geophysically observable, and the equilibria among these phases. The model should be complete in the sense that it accounts for anisotropic properties such as the elastic moduli as well as the usual isotropic thermodynamic properties. Because the relevant range of pressure, temperature and composition is so vast, extrapolation will likely be an essential part of our understanding of mantle thermodynamics for some time. The model should then be sufficiently compact, with a limited number of free parameters, to permit extrapolation with a degree of robustness that may be readily evaluated. It should also be sufficiently flexible as to allow for ready incorporation of additional components, phases and physical behaviour as we continue to learn more about the behaviour of Earth materials at extreme conditions.

In this first paper, we derive the thermodynamic theory and present salient expressions and results that illustrate the scope of our approach, focusing on the physical properties of mantle phases. The second paper will focus on phase equilibria.

2 OUR APPROACH AND PREVIOUS WORK

There have been many previous syntheses of portions of mantle thermodynamics, but none of the scope that we contemplate. Such studies can be divided into two classes on the basis of their primary motivations: (i) to understand phase equilibria (Berman 1988; Fei & Saxena 1990; Holland & Powell 1990; Ghiorso & Sack 1995) and (ii) to understand physical properties (Weidner 1985; Duffy & Anderson 1989). Those focused on phase equilibria typically do not include an account of elastic constants other than the bulk modulus, while those focused on physical properties, including descriptions of the equation of state, or the elastic moduli, typically do not permit computation of phase equilibria.

With the advent of seismic tomography, there has been increasing interest in the development of models that can relate seismic observations to material properties of multiphase assemblages. The key difference between these studies and the theory presented here is our adherence to thermodynamic self-consistency. Thermodynamic self-consistency between phase equilibria and physical properties is exemplified by the Classius–Clapeyron equation, which relates the pressure–temperature slope of phase boundaries to the density and entropy of the phases involved. The physical properties of each phase are also subject to the Maxwell relations. Hybrid models, where a model of physical properties is supplemented by an account of phase equilibria from an independent source, are not self-consistent (Ita & Stixrude 1992; Cammarano *et al.* 2003; Hacker *et al.* 2003). Supplementing phase equilibrium calculations with higher order derivatives of physical properties that do not satisfy the Maxwell relations also violates self-consistency. For example, the model of Sobolev & Babeyko (1994) does not satisfy the relationship between the temperature dependence of the bulk modulus and the pressure dependence of the thermal expansivity. The model of Mattern *et al.* (2005) is thermodynamically self-consistent, but does not permit computation of the shear modulus. The model of Kuskov (1995) is self-consistent in the calculation of phase equilibria, density and bulk sound velocity, but the shear modulus is computed from an independent model.

Our approach, which we have emphasized in our previous work (Stixrude & Bukowinski 1990; Ita & Stixrude 1992; Stixrude & Bukowinski 1993), is based on the concept of fundamental thermodynamic relations (Callen 1960). We take advantage of three important properties of these functions. First, if a thermodynamic potential is expressed as a function of its natural variables, it may be considered a fundamental thermodynamic relation, i.e. it contains all possible thermodynamic information. Secondly, the various thermodynamic potentials are related to one another by Legendre transformations. This means that any of the thermodynamic potentials may be chosen as the fundamental relation and will be equally complete as any other. We will make use of the Gibbs free energy and the Helmholtz free energy, which are related by the Legendre transformation

$$\mathcal{G}(P, T) = \mathcal{F}(V, T) + P(V, T)V. \quad (1)$$

Finally, we take advantage of the first-order homogeneity of thermodynamic functions by writing the fundamental relation in Euler rather than in differential form. This allows us to avoid the limitations of integration along paths that can lead far outside the stability field in mantle applications.

Consideration of elasticity leads us to an essential generalization of textbook thermodynamics. The salient property of the mantle is that it is solid and able to support deviatoric stresses. Elastic waves are then not limited to the bulk sound velocity as in the case of most fluids; our thermodynamic formulation must also encompass shear elasticity. This requires tensorial generalization of familiar concepts such as pressure and volume, and their relationships to entropy and temperature.

3 THEORY

We generalize eq. (1) to one appropriate for crystals. For a solid phase consisting of a solid solution of s species (end-members or phase components),

$$\mathcal{G}(\sigma_{ij}, T) = \sum_{\beta} x_{\beta} \mathcal{G}_{\beta}(\sigma_{ij}, T) + x_{\beta} RT \ln a_{\beta}, \quad (2)$$

where \mathcal{G}_{β} is the Gibbs free energy of pure species β , a_{β} is the activity, R is the gas constant and the stress is related to the pressure by

$$\sigma_{ij} = -P\delta_{ij} + \tau_{ij}, \quad (3)$$

where τ_{ij} is the deviatoric stress. We will assume that the quantity $RT \ln f_{\beta}$ is independent of stress and temperature, where f_{β} is defined by $a_{\beta} = f_{\beta} x_{\beta}$ and x_{β} is the mole fraction. This assumption permits non-ideal enthalpy of solution but neglects the contribution of non-ideality to other physical properties, such as the volume or entropy, because such contributions are small compared with uncertainties in these properties at mantle pressure and temperature (Ita & Stixrude 1992). We have also neglected surface energy, which may be significant for very small grains (~ 1 nm).

Physical properties are related to derivatives of \mathcal{G} ; those that we will discuss further include the entropy \mathcal{S} , volume V , heat capacity C_P , isothermal bulk modulus K , thermal expansivity α and the elastic compliance tensor s_{ijkl} :

$$\mathcal{S} = -\left(\frac{\partial \mathcal{G}}{\partial T}\right)_P = \sum_{\beta} x_{\beta} \mathcal{S}_{\beta} - x_{\beta} R \ln a_{\beta}, \quad (4)$$

$$V = \left(\frac{\partial \mathcal{G}}{\partial P}\right)_T = \sum_{\beta} x_{\beta} V_{\beta}, \quad (5)$$

$$\frac{1}{K} = -\frac{1}{V} \left(\frac{\partial^2 \mathcal{G}}{\partial P^2}\right)_T = \frac{1}{V} \sum_{\beta} x_{\beta} V_{\beta} \frac{1}{K_{\beta}}, \quad (6)$$

$$C_P = -T \left(\frac{\partial^2 \mathcal{G}}{\partial T^2}\right)_P = \sum_{\beta} x_{\beta} C_{P\beta}, \quad (7)$$

$$V\alpha = -\left(\frac{\partial \mathcal{S}}{\partial P}\right)_T = \left(\frac{\partial^2 \mathcal{G}}{\partial P \partial T}\right) = \sum_{\beta} x_{\beta} V_{\beta} \alpha_{\beta}, \quad (8)$$

$$s_{ijkl} = -\frac{1}{V} \left(\frac{\partial^2 \mathcal{G}}{\partial \sigma_{ij} \partial \sigma_{kl}}\right)_{\sigma', T} = \frac{1}{V} \sum_{\beta} x_{\beta} V_{\beta} s_{ijkl\beta}. \quad (9)$$

The subscript on the derivative defining the compliance means stress components except those involved in the derivative are held constant. The elastic moduli are related to the foregoing by

$$\mathbf{c} = \mathbf{s}^{-1} : \quad (10)$$

$$c_{ijkl} = \frac{1}{V} \left(\frac{\partial^2 \mathcal{G}}{\partial S_{ij} \partial S_{kl}}\right)_{P, T} = \frac{1}{V} \left(\frac{\partial^2 \mathcal{F}}{\partial S_{ij} \partial S_{kl}}\right)_{S'_{ij}, T} - P \delta_{kl}^{ij} \neq \frac{1}{V} \sum_{\beta} x_{\beta} V_{\beta} c_{ijkl\beta}, \quad (11)$$

where S_{ij} is the Eulerian strain tensor, discussed further below. The c_{ijkl} are the stress-strain coefficients of Wallace (1972); these are the appropriate elastic constants for the analysis of elastic wave propagation under hydrostatic pre-stress. The second equality relates the moduli to the Helmholtz free energy to which we will turn below. The second strain derivative of the volume is $V \delta_{kl}^{ij}$, with

$$\delta_{kl}^{ij} = -\delta_{ij} \delta_{kl} - \delta_{il} \delta_{jk} - \delta_{jl} \delta_{ik}, \quad (12)$$

and δ_{ij} is the Kronecker delta. The inequality in eq. (11) emphasizes that the elastic moduli of a solid solution can only properly be related to those of its component species via eqs (9) and (10). The adiabatic bulk modulus K_S , adiabatic elastic constant tensor c_{ijkl}^S and isochoric heat capacity C_V are computed from the quantities already given (Davies 1974; Ita & Stixrude 1992).

We will be particularly interested in the bulk modulus and the shear modulus G , which for an isotropic material obey the following relations (Nye 1985):

$$3K = \frac{3}{s_{ijkl} \delta_{ij} \delta_{kl}} = \frac{c_{ijkl} \delta_{ij} \delta_{kl}}{3}, \quad (13)$$

$$G = \frac{1}{s_{44}} = \frac{1}{2(s_{11} - s_{12})} = c_{44} = \frac{c_{11} - c_{12}}{2}, \quad (14)$$

where we have adopted the Einstein summation convention and used Voigt notation in eq. (14). The first equality in eq. (13) holds for materials of any symmetry. From eq. (9),

$$\frac{1}{G} = \frac{1}{V} \sum_{\beta} x_{\beta} V_{\beta} \frac{1}{G_{\beta}}. \quad (15)$$

For anisotropic phases, a class of materials that includes all crystals, the shear modulus is interpreted as that of an isotropic polycrystalline aggregate upon which rigorous bounds can be placed (Watt *et al.* 1976).

To specify the form of the Gibbs free energy of the species, \mathcal{G}_{β} , we follow previous work and make use of the Legendre transformation (eq. 1). The Helmholtz free energy may be written

$$\mathcal{F}(E_{ij}, T) = \mathcal{F}_0(0, T_0) + \mathcal{F}_c(E_{ij}, T_0) + \mathcal{F}_q(E_{ij}, T) - \mathcal{F}_q(E_{ij}, T_0), \quad (16)$$

where the terms are respectively the reference value at the natural configuration and the contributions from compression at ambient temperature (the so-called cold part), and lattice vibrations in the quasi-harmonic approximation. These contributions are expected to be most important for mantle phases. We will discuss other contributions that are more important for phase equilibria in Paper II including anharmonic, magnetic, electronic and disordering contributions. The E_{ij} is the Eulerian finite strain relating the natural state at ambient conditions with material points located at coordinates $a_i = (a_1, a_2, a_3)$, to the final state with coordinates x_i :

$$E_{ij} = \frac{1}{2} \left(\delta_{ij} - \frac{\partial a_i}{\partial x_k} \frac{\partial a_j}{\partial x_k} \right). \quad (17)$$

Thermodynamic quantities are related to the S_{ij} (eqs 4–11), which relate the final state to the initial or pre-stressed state with coordinates X_i :

$$S_{ij} = \frac{1}{2} \left(\delta_{ij} - \frac{\partial X_i}{\partial x_k} \frac{\partial X_j}{\partial x_k} \right). \quad (18)$$

We assume that the initial state is one of hydrostatic stress, appropriate to the interior of the Earth, and that the final state differs slightly from the initial state, corresponding to the small amplitude of seismic waves. Our point of view differs slightly from that adopted by Davies (1974). We view the natural configuration as that at ambient pressure and temperature, whereas Davies (1974) assumed a different natural configuration for each temperature, such that the pressure is zero for each natural configuration. Our natural configuration therefore corresponds to the master configuration of Thurston (1965).

We adopt the following form for the Helmholtz free energy (eq. 16):

$$\begin{aligned} \rho_0 \mathcal{F} = & \rho_0 \mathcal{F}_0 + \frac{1}{2} b_{ijkl}^{(1)} E_{ij} E_{kl} - \frac{1}{6} b_{ijklmn}^{(2)} E_{ij} E_{kl} E_{mn} + \frac{1}{24} b_{ijklmnop}^{(3)} E_{ij} E_{kl} E_{mn} E_{op} + \dots \\ & + \rho_0 k T \sum_{\lambda} \ln \left\{ 1 - \exp \left[- \frac{h \nu_{\lambda}(E_{ij})}{k T} \right] \right\} - \rho_0 k T_0 \sum_{\lambda} \ln \left\{ 1 - \exp \left[- \frac{h \nu_{\lambda}(E_{ij})}{k T_0} \right] \right\}, \end{aligned} \quad (19)$$

which is the generalization to anisotropic strain of that used in our previous work (Ita & Stixrude 1992). The cold part is a Taylor series expansion in the Eulerian finite strain, E_{ij} , and the quasi-harmonic part is exact as written and includes a sum over all vibrational modes λ , with the dependence of the frequencies ν_{λ} on strain made explicit. The density $\rho = 1/V$ and k is the Boltzmann constant. Two comments on notation: (i) the choice of sign conforms to standard usage because E_{ij} is positive on expansion, while the isotropic finite strain f , discussed below, is usually defined positive on compression; (ii) the parenthetical superscripts, also used by Davies (1974), provide a convenient way of distinguishing among the coefficients when alternating between standard and Voigt notation.

We find the equation of state and the elastic constants by taking the appropriate strain derivatives of eq. (19) and evaluating in the initial state:

$$\rho_0 \mathcal{F} = \rho_0 \mathcal{F}_0 + \frac{1}{2} b_{iikk}^{(1)} f^2 + \frac{1}{6} b_{iikkmm}^{(2)} f^3 + \frac{1}{24} b_{iikkmmoo}^{(3)} f^4 + \dots + \rho_0 \Delta \mathcal{F}_q, \quad (20)$$

$$P = -\frac{1}{3} \sigma_{ij} \delta_{ij} = \frac{1}{3} (1 + 2f)^{5/2} \left[b_{iikk}^{(1)} f + \frac{1}{2} b_{iikkmm}^{(2)} f^2 + \frac{1}{6} b_{iikkmmoo}^{(3)} f^3 + \dots \right] + \gamma \rho \Delta \mathcal{U}_q, \quad (21)$$

$$\begin{aligned} c_{ijkl} = & (1 + 2f)^{7/2} \left[b_{ijkl}^{(1)} + b_{ijklmm}^{(2)} f + \frac{1}{2} b_{ijklmmoo}^{(3)} f^2 + \dots \right] - P_c \delta_{kl}^{ij} \\ & + \left[\gamma_{ij} \gamma_{kl} + \frac{1}{2} (\gamma_{ij} \delta_{kl} + \gamma_{kl} \delta_{ij}) - \eta_{ijkl} \right] \rho \Delta \mathcal{U}_q - \gamma_{ij} \gamma_{kl} \rho \Delta (C_V T). \end{aligned} \quad (22)$$

In deriving eqs (20)–(22), we have made use of the strain–strain derivatives relating E_{ij} to S_{ij} (Thomsen 1972) and have assumed that the finite strain in the initial state is isotropic with

$$E_{ij} = -f \delta_{ij}, \quad (23)$$

$$f = \frac{1}{2} \left[\left(\frac{\rho}{\rho_0} \right)^{2/3} - 1 \right], \quad (24)$$

$\mathcal{F}_q, \mathcal{U}_q$ are the quasi-harmonic free energy and internal energy, and the Δ notation indicates the change in these quantities from the reference temperature.

The coefficients appearing in eqs (20)–(22) may be found by evaluating eq. (22) and its pressure derivatives at ambient conditions,

$$b_{ijkl}^{(1)} = c_{ijkl0}, \quad (25)$$

$$b_{ijklmm}^{(2)} = 3K_0 \left(c'_{ijkl0} + \delta_{kl}^{ij} \right) - 7c_{ijkl0}, \quad (26)$$

$$b_{ijklmmoo}^{(3)} = 9K_0^2 c''_{ijkl0} + 3K_0 \left(c'_{ijkl0} + \delta_{kl}^{ij} \right) (3K'_0 - 16) + 63c_{ijkl0}, \quad (27)$$

from which we may determine the scalar coefficient by applying the Einstein summation convention,

$$b_{iikk}^{(1)} = 9K_0, \quad (28)$$

$$b_{iikkmm}^{(2)} = 27K_0 (K'_0 - 4), \quad (29)$$

$$b_{iikkmmoo}^{(3)} = 81K_0 \left[K_0 K''_0 + K'_0 (K'_0 - 7) + \frac{143}{9} \right]. \quad (30)$$

Previous studies have formed an alternative expression for the cold contribution to the elastic constants by combining eqs (21) and (22), eliminating the cold pressure P_c . In order to maintain thermodynamic self-consistency, we retain all terms in the elastic constants and pressure that originate from the same order in the free energy expansion (eq. 20). The expression for the cold part of the moduli to third order is then

$$c_{ijkl} = (1 + 2f)^{5/2} \left\{ c_{ijkl0} + (3K_0 c'_{ijkl0} - 5c_{ijkl0})f + \left[6K_0 c'_{ijkl0} - 14c_{ijkl0} - \frac{3}{2}K_0 \delta_{kl}^{ij} (3K'_0 - 16) \right] f^2 \right\}. \quad (31)$$

To illustrate the thermodynamic consistency of eq. (31), we evaluate the bulk modulus via eq. (13),

$$K = (1 + 2f)^{5/2} \left[K_0 + (3K_0 K'_0 - 5K_0)f + \frac{27}{2}(K_0 K'_0 - 4K_0)f^2 \right] + (\gamma + 1 - q)\gamma\rho\Delta\mathcal{U}_q - \gamma^2\rho\Delta(C_V T), \quad (32)$$

which agrees with the expression to third order derived from a purely isotropic thermodynamic analysis (Ita & Stixrude 1992). The shear modulus evaluated from eq. (31),

$$G = (1 + 2f)^{5/2} \left[G_0 + (3K_0 G'_0 - 5G_0)f + \left(6K_0 G'_0 - 24K_0 - 14G_0 + \frac{9}{2}K_0 K'_0 \right) f^2 \right] - \eta_S \rho \Delta\mathcal{U}_q, \quad (33)$$

differs from that found in previous studies (Sammis *et al.* 1970; Davies & Dziewonski 1975) that truncated eq. (31) after the linear f term, resulting in elastic constants that are thermodynamically inconsistent with the pressure and the Helmholtz free energy at order f^2 . In eq. (33), we have introduced the quantity η_S , which we now discuss further.

The quasi-harmonic parts of eqs (20)–(22) involve the anisotropic generalization of the Grüneisen parameter and its strain derivative,

$$\gamma_{ij} = -\frac{1}{v_\lambda} \frac{\partial v_\lambda}{\partial S_{ij}}, \quad (34)$$

$$\eta_{ijkl} = \frac{\partial \gamma_{ij}}{\partial S_{kl}}, \quad (35)$$

where we have adopted the Grüneisen approximations that γ_{ij} and η_{ijkl} are the same for all vibrational modes λ . For an isotropic material,

$$\gamma_{ij} = \gamma \delta_{ij}, \quad (36)$$

$$\eta_{ijkl} = \gamma q \delta_{ij} \delta_{kl} + \eta_S \left(\delta_{ik} \delta_{jl} + \delta_{il} \delta_{jk} - \frac{2}{3} \delta_{ij} \delta_{kl} \right), \quad (37)$$

where

$$\gamma = V \left(\frac{\partial P}{\partial \mathcal{U}} \right)_V, \quad (38)$$

$$q = \left(\frac{\partial \ln \gamma}{\partial \ln V} \right) \quad (39)$$

and η_S is the shear strain derivative of γ . In deriving eq. (33), we have assumed that the η tensor is isotropic and can be divided into volume (γq) and shear (η_S) sensitive parts according to eq. (37).

We assume that the frequencies follow a Taylor series expansion in the Eulerian finite strain (Leibfried & Ludwig 1961; Thomsen 1972; Davies 1974),

$$v_\lambda^2 = v_{\lambda 0}^2 \left[1 - a_{ij}^{(1)} E_{ij} + \frac{1}{2} a_{ijkl}^{(2)} E_{ij} E_{kl} + \dots \right], \quad (40)$$

where we have again invoked the Grüneisen approximations. Taking the appropriate strain derivatives, evaluating at isotropic finite strain and suppressing the vibrational mode index, λ ,

$$v^2 = v_0^2 \left[1 + a_{ii}^{(1)} f + \frac{1}{2} a_{iikk}^{(2)} f^2 + \dots \right], \quad (41)$$

$$\gamma_{ij} = \frac{1}{2} \frac{v_0^2}{v^2} (2f + 1) \left[a_{ij}^{(1)} + a_{iikk}^{(2)} f \right], \quad (42)$$

$$\eta_{ijkl} = 2\gamma_{ij}\gamma_{kl} - \gamma_{jk}\delta_{il} - \gamma_{ik}\delta_{jl} - \frac{1}{2} \frac{v_0^2}{v^2} (2f + 1)^2 a_{ijkl}^{(2)}, \quad (43)$$

which reduce for an isotropic material to

$$\gamma = \frac{1}{6} \frac{v_0^2}{v^2} (2f + 1) \left[a_{ii}^{(1)} + a_{iikk}^{(2)} f \right], \quad (44)$$

$$\eta_V = \gamma q = \frac{1}{9} \left[18\gamma^2 - 6\gamma - \frac{1}{2} \frac{v_0^2}{v^2} (2f + 1)^2 a_{iikk}^{(2)} \right], \quad (45)$$

$$\eta_S = -\gamma - \frac{1}{2} \frac{v_0^2}{v^2} (2f + 1)^2 a_S^{(2)}. \quad (46)$$

The coefficients are related to values at ambient conditions as follows:

$$\begin{aligned} a_{ij}^{(1)} &= 2\gamma_{ij0}, & a_{ii}^{(1)} &= 6\gamma_0, \\ a_{ijkl}^{(2)} &= 4\gamma_{ij0}\gamma_{kl0} - 2\gamma_{jk0}\delta_{il} - 2\gamma_{ik0}\delta_{jl} - 2\eta_{ijkl0}, \\ a_{iikk}^{(2)} &= -12\gamma_0 + 36\gamma_0^2 - 18q_0\gamma_0, \\ a_S^{(2)} &= -2\gamma_0 - 2\eta_{S0}. \end{aligned} \quad (47)$$

We will also examine an alternative expression for the volume dependence of the frequencies that has been used extensively in the literature:

$$v = v_0 \exp\left(\frac{\gamma_0 - \gamma}{q}\right), \quad (48)$$

$$\gamma = \gamma_0 \left(\frac{\rho}{\rho_0}\right)^{-q}, \quad (49)$$

where q is typically taken as constant, although variable q , via a further logarithmic volume derivative (q'), has also been discussed (Jeanloz 1989).

Our development follows closely that of Davies (1974). The cold contributions in eqs (20)–(22) are equivalent to those derived in that study, as are the quasi-harmonic terms evaluated at zero strain. Our approach differs in the treatment of the strain dependence of the quasi-harmonic terms. While Davies (1974) included the quasi-harmonic contribution only in its effect on the lowest order coefficient in the finite strain expansion, our approach is more akin to the Mie–Grüneisen formulation that we have used in our previous work, retaining the complete quasi-harmonic term separately from the cold contribution.

4 TESTS OF THE THEORY

One of the most important developments since the work of Davies (1974) is that the theory may now be tested extensively against experimental data and first principles calculations. We will examine the choice of finite strain variables (Eulerian versus Lagrangian), the degree of anisotropy in the Grüneisen and η tensors, the choice of volume dependence of the Grüneisen parameter, q , and η_S , and the choice of the form of the vibrational density of states.

The rationale for testing our thermodynamic theory against first principles calculations, as well as experiments, is three-fold:

- (i) first principles calculations are independent of experiments (no free parameters) and yet agree well with measurements where comparisons are possible;
- (ii) these quantum mechanical calculations are completely independent of the thermodynamic development outlined above and free of the approximations that underly it, such as finite strain theory;
- (iii) first principles calculations have explored the behaviour of the shear modulus and the Grüneisen parameter over a much wider range of pressure and temperature than experiments.

The differences between alternative finite strain formulations or different approximations for q only become apparent at large compressions. Also for this reason, we focus our tests of these aspects of our thermodynamic development on phases of the lower mantle.

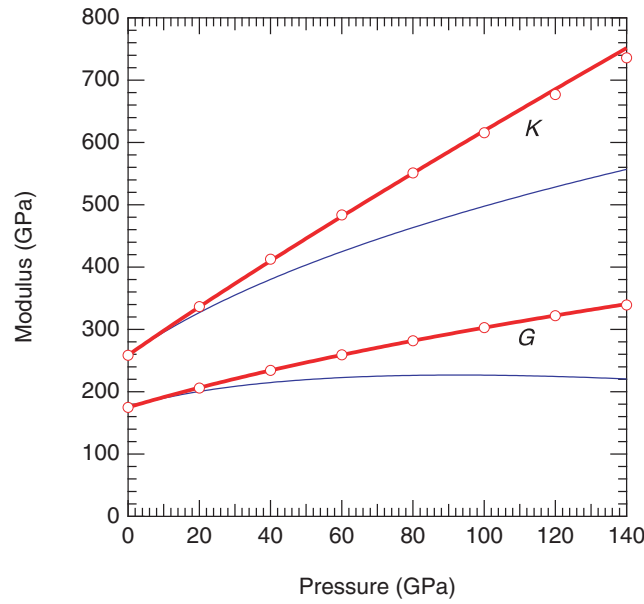


Figure 1. (Bold lines) Eulerian third-order finite strain versus (thin lines) Lagrangian third-order finite strain expressions compared with (symbols) first principles results from Karki *et al.* (1997) for the isothermal bulk modulus (K) and the shear modulus (G) of MgSiO_3 perovskite. For the purposes of this comparison, the finite strain curves were calculated using values of $K_0 = 259$, $G_0 = 175$, $K'_0 = 4.0$ and $G'_0 = 1.7$ taken from the first principles study.

4.1 Finite strain variables

The Eulerian finite strain expansion is substantially superior to the Lagrangian (Fig. 1) in representing the bulk and shear moduli. First principles theoretical results for MgSiO_3 perovskite are described by a third-order Eulerian finite strain expansion to within 1 per cent for the shear modulus and 3 per cent for the bulk modulus. Use of the thermodynamically self-consistent expression (eqs 32 and 33) is important: neglect of the f^2 term leads to values of the shear modulus that are 8 per cent greater at high pressure. For the bulk modulus, the third-order expansion deviates systematically at the highest pressures indicating either a significant fourth-order term, or systematic inaccuracies in the first principles theoretical results. The agreement with the third-order Lagrangian finite strain expansion is poor by comparison: disagreements reach 34 and 24 per cent for shear and bulk moduli respectively at the highest pressures.

Our findings are consistent with previous studies of the equation of state. The rapid convergence of the Eulerian equation of state may be rationalized by recognizing that for $K'_0 = 4$, a value typical of a wide range of solids, the third-order term vanishes. The convergence of the Eulerian expansion for the elastic constants may be understood in a similar way (Karki *et al.* 2001). The coefficients of the third-order term vanish when

$$c'_{ijkl0} = \frac{7}{3} \frac{c_{ijkl0}}{K_0} - \delta_{kl}^{ij}. \quad (50)$$

Experimental and first principles theoretical values deviate from this trend by amounts that are similar to measured deviations of K'_0 from 4. For some minerals, the fourth-order term appears to be significant. For example, accurate description of the acoustic velocities of orthopyroxene (Webb & Jackson 1993; Flesch *et al.* 1998) and of forsterite (Zha *et al.* 1998), require fourth-order terms in the Eulerian finite strain expansion, although in the case of forsterite, a third-order expansion suffices within the thermodynamic stability field.

4.2 Anisotropy of γ and η tensors

Analysis of available experimental data suggests that the anisotropy of the Grüneisen tensor, when it is permitted by symmetry, is small. The individual components of the Grüneisen tensor may be related to experimentally measured quantities via (Davies 1974):

$$\gamma_{ij} = \frac{c_{ijkl}^S \alpha_{kl}}{\rho C_p}. \quad (51)$$

All the quantities appearing on the right-hand side are available at elevated temperature for three non-cubic mantle species: forsterite, fayalite and corundum. For all three materials, the individual components of γ are indistinguishable within mutual uncertainty, despite substantial anisotropy in the thermal expansivity tensor α_{ij} and c_{ijkl} : components differ by no more than 0.2 (2), 0.3 (5) and 0.03 (26) for the three species respectively (estimated two-sigma uncertainties in parentheses). We can understand why γ is more isotropic than either of the tensorial quantities on the right-hand side of eq. (51) by observing that the crystallographic direction with greatest thermal expansion tends to correspond to the direction with the softest longitudinal elastic constant.

Available experimental data suggest that anisotropy in η_{ijkl} may be resolvable for some species and not for others (Fig. 2). There are four cubic species for which the elastic constants have been measured at high temperature. Assuming isotropic η_{ijkl} , with individual components

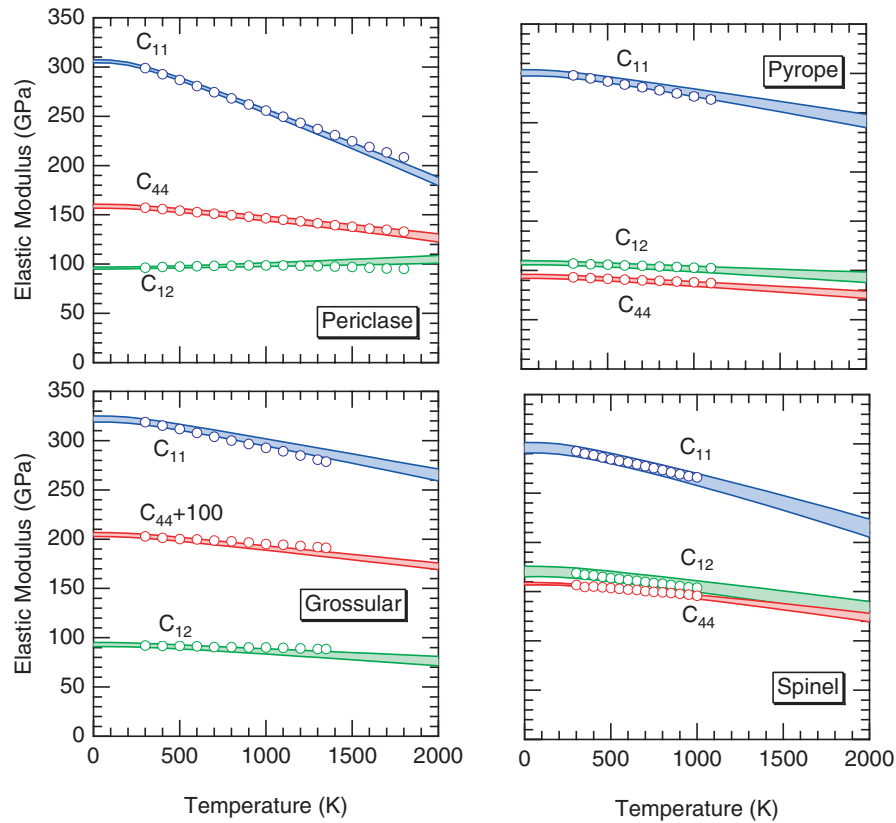


Figure 2. Elastic moduli of cubic crystals from (symbols) experiments and (lines) finite strain theory with elements of the isotropic eta tensor given by eq. (37). Shading represents propagated uncertainties in the calculated curves. See Table 1 for parameter values, uncertainties and experimental references.

Table 1. Anisotropic properties of cubic phases.

	c_{11}	c_{12}	c_{44}	c'_{11}	c'_{12}	c'_{44}	η_{11}	η_{12}	η_{44}	Ref.
Spinel	292.2 (52)	168.7 (52)	156.5 (10)	5.59 (10)	5.69 (10)	1.44 (10)	6.5 (10)	1.0 (8)	2.7 (6)	1,2
Pyrope	298.0 (30)	107.0 (20)	93.0 (20)	5.36 (40)	3.21 (30)	1.29 (30)	2.8 (7)	0.7 (6)	1.0 (3)	3,4
Grossular	318.9 (30)	92.2 (20)	102.9 (20)	6.29 (10)	5.42 (10)	2.12 (10)	3.7 (5)	-1.2 (5)	2.4 (2)	1,5
Periclase	299.0 (15)	96.4 (10)	157.1 (20)	9.05 (20)	1.34 (30)	0.84 (30)	5.4 (3)	0.7 (3)	2.3 (2)	1,4

References: 1, Anderson & Isaak (1995); 2, Yoneda (1990); 3, Sinogeikin & Bass (2002b); 4, Sinogeikin & Bass (2000); 5, Conrad *et al.* (1999).

Units: GPa for elastic moduli, others dimensionless. Uncertainties of last reported digits in parentheses.

given by eq. (37) and parameters from Table A1, and experimentally measured elastic moduli and pressure derivatives (Table 1), we find perfect agreement with the high-temperature data for spinel and pyrope. For periclase, the agreement is excellent up to a temperature of approximately 1300 K, where c_{11} and c_{12} begin to show substantial curvature. For grossular, isotropic η_{ijkl} disagrees systematically with the experimentally determined trend. For this mineral then, anisotropy is apparently resolvable. We have determined best-fitting anisotropic values for grossular as follows: $\eta_{11} = 5.7$, $\eta_{12} = -2.8$, $\eta_{44} = 0.8$, which may be compared with the isotropic values in Table 1.

4.3 Volume dependence of γ , q and η

We find that eq. (44) provides an excellent description of the volume dependence of γ that is superior to the more usual assumption $q = \text{constant}$ (eq. 49). We compare to first principles theoretical results of MgSiO₃ perovskite and MgO periclase (Fig. 3). The first principles results show that γ decreases with compression and that the rate of decrease itself decreases with compression. This pattern means that q is positive and that it decreases with compression. The decrease in q with compression is significant. If we assume that q is constant, we underestimate γ by 20 per cent at 25 per cent compression. Previous theoretical and experimental studies have also found that q decreases with compression (Agnon & Bukowinski 1990; Speziale *et al.* 2001). It is worth emphasizing that the finite strain formulation (eq. 44) requires no additional free parameter to describe the volume dependence of γ and q beyond their values in the natural state.

To our knowledge, the volume dependence of η_{ijkl} has not previously been analysed. For isotropic η , the volume dependence of η_V is specified by the volume dependence of γ and q , because $\eta_V = \gamma q$. We find that (eq. 46) is able to reproduce the influence of compression on dG/dT as determined by first principles calculations (Fig. 4). In contrast, if we assume that η_S is a constant, or that it is proportional to

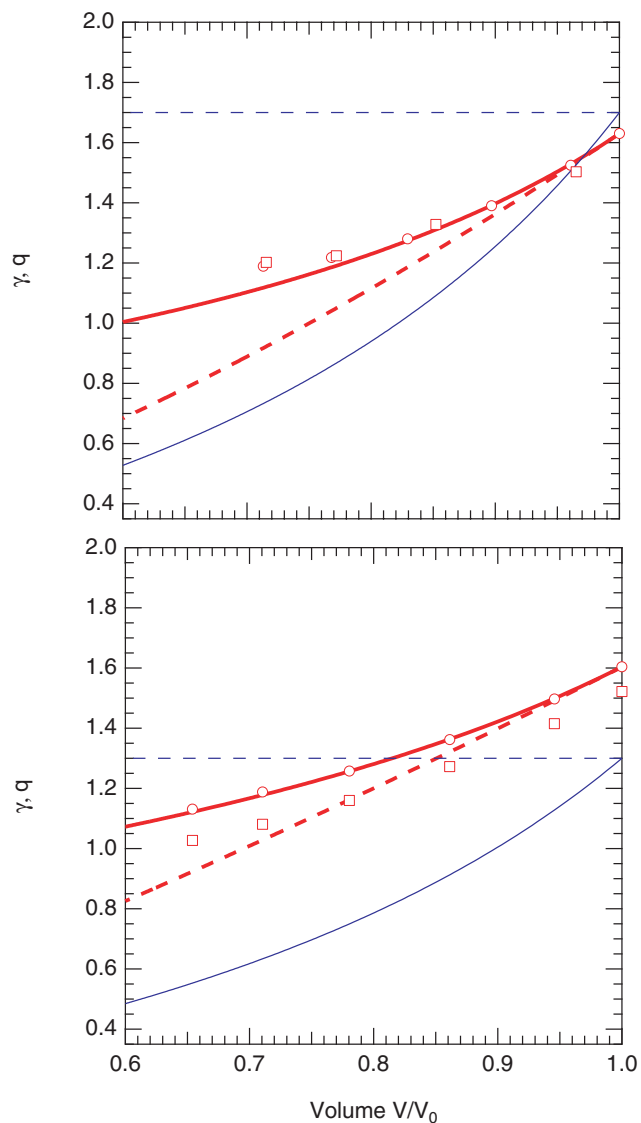


Figure 3. Grüneisen parameter from (symbols) first principles calculations compared with (solid lines) finite strain theory and (dashed lines) constant q approximation for MgSiO_3 perovskite (top) and MgO periclase (bottom). Bold lines show the Grüneisen parameter and thin lines show q . First principles results are at 1000 K from (circles) Karki *et al.* (2000b) and (squares) Oganov & Dorogokupets (2003a) for periclase, and (circles) Karki *et al.* (2000a) and (squares) Oganov *et al.* (2001a) for perovskite. For perovskite, $V_0 = 168.27 \text{ \AA}^3$ per unit cell (Karki *et al.* 2000b), and for periclase $V_0 = 77.24 \text{ \AA}^3$ per unit cell (Karki *et al.* 2000b). Lines are calculated assuming the following values taken from the first principles calculations for the purposes of this comparison: $\gamma_0 = 1.63$ and $q_0 = 1.7$ for perovskite, and $\gamma_0 = 1.60$ and $q_0 = 1.3$ for periclase. In the case of periclase, the two first principles calculations disagree in the value of γ_0 but show the same functional form.

η_V , we find very poor agreement with the first principles results. The simple assumption that η_S scales with the volume, adopted by Stixrude & Lithgow-Bertelloni (2005), is remarkably successful, at least in the case of MgSiO_3 perovskite, in capturing the behaviour of the full theory.

4.4 Vibrational density of states

A number of studies have shown that the Debye model is a useful approximation even when it does not capture the form of the vibrational density of states in detail (Stixrude & Bukowinski 1990; Jackson & Rigden 1996; Shim & Duffy 2000). The reason that such a simple one-parameter description can be successful is that thermodynamic properties do not depend on the vibrational density of states, but on integrals over the vibrational spectrum. As a result, many thermodynamic properties are not sensitive to the detailed form of the vibrational density of states, except at very low temperatures.

The idea that thermochemical properties are increasingly insensitive to the form of the vibrational density of states with increasing temperature is captured by the theory of Barron *et al.* (1957), which yields the exact expression for the quasi-harmonic vibrational entropy

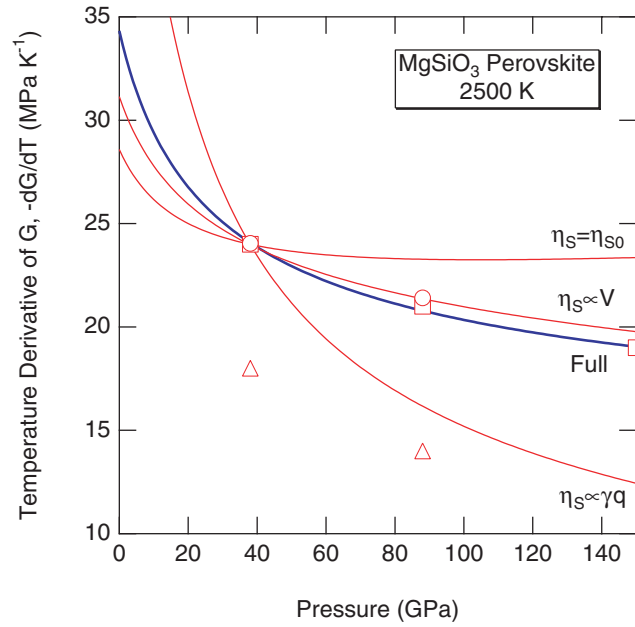


Figure 4. Temperature derivative of the shear modulus from density functional theory (squares) Wentzcovitch *et al.* (2004), (circles) Oganov *et al.* (2001b), and from a more approximate ab initio model (Potential Induced Breathing; triangles) Marton & Cohen (2002) and (lines) finite strain theory for several different approximations of the volume dependence of η_S : (bold) full finite strain theory, (light lines) η_S arbitrarily assumed to be constant ($\eta_S = \eta_{S0}$), proportional to the volume, V , or proportional to η_V . The value of η_{S0} for each curve is set so that it passes through the first principles point at 38 GPa.

per atom,

$$\mathcal{S} = 3R \left\{ \frac{4}{3} - \ln \frac{\theta(0)}{T} + \frac{3B_2}{10 \cdot 2!} \left[\frac{\theta(2)}{T} \right]^2 - \frac{9B_4}{28 \cdot 4!} \left[\frac{\theta(4)}{T} \right]^4 + \dots \right\}, \quad (52)$$

where B_n are the Bernoulli numbers and the n^{th} moment of vibrational density of states $\theta(n)$ is defined in such a way that all moments are equal for a Debye spectrum. Similar expressions for the internal energy (enthalpy) and heat capacity show the expected approach to the Dulong–Petit limit as $1/T \rightarrow 0$; only the entropy depends on the vibrational density of states to lowest order. For $\theta(n) \approx 750$ K and $T \approx 1000$ K, the T^{-2} and higher order terms account for less than 1 per cent of the total.

We have found that thermochemical properties of many mantle phases differ insignificantly from those given by a Debye spectrum from room temperature to mantle temperatures (Fig. 5). The comparison is based on an effective Debye temperature that is fit to the experimental determination of the entropy at 1000 K and can thus be related to $\theta(0)$. Differences between the Debye and experimentally determined entropy are less than $1.5 \text{ J mol}^{-1} \text{ atom}^{-1} \text{ K}^{-1}$ for minerals with very non-Debye-like vibrational spectra (e.g. anorthite) to better than experimental precision for Debye-like solids such as corundum.

More complex models of the vibrational density of states may provide a better match to thermochemical data, but at the cost of additional free parameters that become increasingly uncertain at elevated pressure. The Kieffer (1980) model generally, although not always, matches data better than the one-parameter effective Debye model (Fig. 5). In this study, we will prefer the simpler effective Debye model, although our approach will accommodate additional experimental information on the full vibrational density of states as this continues to be gathered (Chopelas 1999; Chaplot *et al.* 2002).

5 MODEL AND PARAMETER ESTIMATION

Based on our theoretical development and discussion, we explore further the properties of the following thermodynamic model of mantle species: the fundamental relation (eq. 20) truncated after the cubic term for an isotropic material with vibrational density of states approximated by the Debye model and volume dependence given by the finite strain expansion (eq. 41). The equation of state, and bulk and shear moduli are calculated via strain derivatives of the fundamental relation (eqs 21, 32 and 33).

The model contains eight material-specific parameters that are required to compute physical properties: V_0 , K_0 , K'_0 , θ_0 , γ_0 , q_0 , G_0 , G'_0 and η_{S0} . Most or all of these parameters are now constrained by experimental measurements for at least one species of most major mantle phases. In order to compute phase equilibria, \mathcal{F}_0 and regular solution parameters will also be required and will be discussed at length in Paper II.

We perform an iterative global least-squares inversion of experimental data for the values of the parameters of each mantle species (Table A1, Appendix A). We supplement experimental measurements with the results of first principles calculations for properties that have

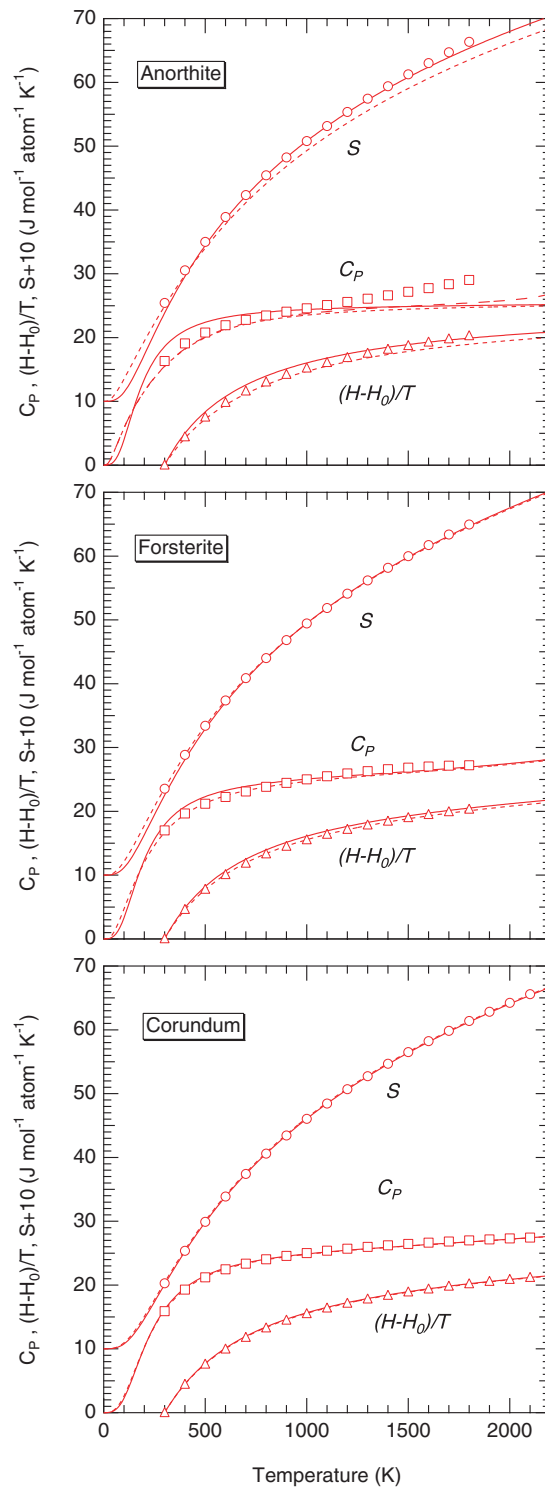


Figure 5. Experimentally derived (Robie & Hemingway 1995) entropy (circles), heat capacity (squares) and enthalpy function (triangles) compared with (solid lines) Debye model with effective Debye temperature fit to the entropy at 1000 K, and (short dashed) the model of Kieffer (1980). For anorthite, the long dashed line shows the influence of cation disorder on the heat capacity according to the model of Holland & Powell (1998). The entropy is shifted upwards for clarity. Debye model calculations are based on parameters in Table A1; Kieffer model calculations are based on the same parameters (except for θ_0) and the Grüneisen approximations.

not yet been measured experimentally. When neither experimental nor first principles results exist, we rely on systematic relationships, some of which are summarized in Fig. 6. The global inversion is discussed in more detail in Appendix A.

To provide a means of gauging the robustness of the model parameters determined from the global inversion, we analyse: (i) the sensitivity of various experimentally measured quantities to the values of the parameters, and (ii) the physics underlying each parameter and estimates

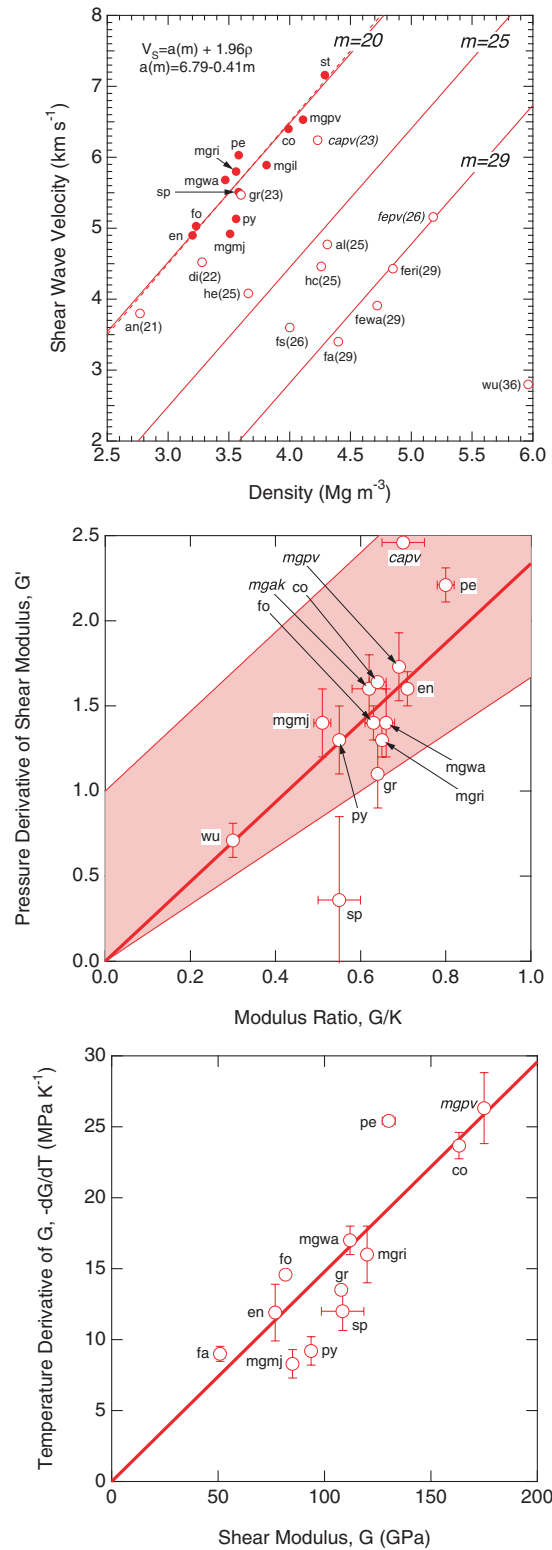


Figure 6. Systematic relations used to estimate parameter values for which no experimental or first principles constraints exist: symbols represent experimental data or first principles results (italicized labels). (Top) Experimental shear wave velocity and density data for species with (solid symbols) mean atomic weight $\bar{m} = 20 \pm 1$ and (open) other mean atomic weights as indicated in parentheses. The best-fitting equation to the data set is shown in the inset and illustrated for three values of the mean atomic weight as indicated. The dashed curve is from Anderson *et al.* (1968) for $\bar{m} = 20$. (Middle) Experimental data and first principles results compared with (thin solid lines and shading) the relationships implied by second-order Eulerian finite strain theory according to (upper) eq. (A3) and (lower) eq. (A4), and (thick solid) the best-fitting direct relationship to the data. (Bottom) Experimental data and first principles results compared with (line) the best-fitting direct relationship.

of their most likely values. We focus our analysis on θ_0 , γ_0 , q_0 and η_{S0} because it is difficult to measure these directly, although, as we will show, each may be related to commonly measured quantities. The value of these illustrations is primarily heuristic and supplements the full global inversion.

Before proceeding with our heuristic analysis, it is worth emphasizing the importance of functional form in the construction of a thermodynamic model. It may be tempting to describe the T dependence of the elastic moduli as a Taylor series in T because the coefficients may be thought of as being more directly related to experimental measurements than the thermal parameters of our model. Aside from the issue of thermodynamic self-consistency, such a series is unlikely to converge rapidly for the same reason that a Taylor series expansion in $V(P, T)$ does not: the moduli depend linearly on temperature only over a limited range of T and the P – T cross-derivative as well as higher order derivatives are non-zero. So, the choice of temperature derivatives of K and G as model parameters would necessitate at least four additional model parameters to describe the non-linearity of the temperature dependence and the non-zero pressure–temperature cross-derivatives. We have argued above and show further below that our formulation is able to capture both of these features of the P and T dependence of the moduli without recourse to additional parameters. Our more compact formulation leads to extrapolation beyond the experimentally measured regime that, while necessarily uncertain, is at least physically reasonable and non-divergent, as we have argued above.

5.1 Parameter sensitivity

We anticipate that thermochemical quantities (C_P , S , H) will be most sensitive to θ_0 as can be seen from the theory of Barron *et al.* (1957; e.g. eq. 52). Dependence on γ_0 and q_0 will be much weaker because their only influence is via the effect of thermal expansion on θ and on the correction from isochoric to isobaric heat capacity. Thermal expansion will be most sensitive to γ_0 as can be seen from eq. (21) and realizing that, at temperatures where the thermal expansion is large, the thermal energy is near the Dulong–Petit limit. Thermal expansion will also be influenced by q_0 , because this parameter controls the rate at which γ varies upon expansion. High-temperature measurements of the bulk modulus are also sensitive to q_0 (eq. 32). All of the properties discussed so far are independent of the value of η_{S0} which influences only shear elasticity (eq. 33). The shear modulus at elevated temperature is most sensitive to η_{S0} , and secondarily to γ_0 and q_0 , and G'_0 . These anticipated relationships are borne out by numerical calculation (Fig. 7).

5.2 Analysis of likely parameter values

We anticipate the value of θ_0 via eq. (52). We expect that the effective Debye temperature found by fitting to experimental measurements of the entropy should be very similar to $\theta(0)$, which may be independently estimated from models of the vibrational density of states. For a range of values of the vibrational entropy from 33 (stishovite) to 46 J mol^{−1} atom^{−1} K^{−1} (fayalite, assuming $R \ln 5$ magnetic entropy per Fe), we anticipate values of $\theta \approx 1000$ –600 K. This range is similar to that found in previous studies of mantle minerals (Watanabe 1982; Ita & Stixrude 1992).

The Grüneisen parameter is, from eq. (38),

$$\gamma = \frac{\alpha K_T}{C_V \rho}. \quad (53)$$

We may anticipate values of γ_0 , by plotting numerator against denominator (Fig. 8). The uncertainties in the numerator are sufficiently large that the approximation $C_V \approx 3R$ per atom does not increase the error significantly. From this analysis, we anticipate values that fall between 0.5 and 1.5, and uncertainties of order 0.1. This range is very similar to the range of Grüneisen parameters that have been proposed in the literature for mantle phases (Watanabe 1982; Ita & Stixrude 1992).

The value of q_0 may be approximated (Anderson 1995):

$$q \approx \delta_T - K'_0 + 1, \quad (54)$$

where $\delta_T = -(\alpha K)^{-1}(\partial K/\partial T)_P$. Plotting δ_T against K'_0 , we anticipate values of q falling mostly within the range 1–3 (Fig. 8). Our analysis shows that the precision of existing experimental data is sufficient to distinguish the value of q_0 from unity for many mantle species. The expectation that $q \approx 1$ is based on Hugoniot and other high-pressure data, primarily on materials atypical of the mantle (Carter *et al.* 1971; Boehler & Ramakrishnan 1980). As Shim & Duffy (2000) have pointed out, static or dynamic equation of state data must cover a wide range of P – T conditions in order to constrain q effectively. Values of $q_0 > 2$ have been found in previous analyses of shock wave data of stishovite (Luo *et al.* 2002), and static P – V – T data for MgSiO₃ perovskite (Stixrude *et al.* 1992; Shim & Duffy 2000) and ringwoodite (Katsura *et al.* 2004).

The value of η_{S0} is most simply estimated by

$$\frac{\eta_S}{\gamma} \approx \delta_G - G'_0, \quad (55)$$

where $\delta_G \equiv -(\partial G/\partial T)_P (\alpha K_T)^{-1}$. From a plot of δ_G versus G'_0 , we anticipate values of the ratio that fall mostly in the range 1–3 (Fig. 8). As the equation shows, positive values mean that the non-dimensional temperature derivative of the shear modulus exceeds the non-dimensional pressure derivative. On this basis, the shear modulus may be considered to be more sensitive to temperature than to pressure, i.e. $\eta_S/\gamma > 0$ means that $\delta_G = -(G/K) (\partial \ln G/\partial \ln V)_P$ is greater than $G' = -(G/K) (\partial \ln G/\partial \ln T)_T$. This pattern is similar to the bulk modulus for which values of $q > 1$ also reveal a greater sensitivity to temperature than to pressure, i.e. that $\delta_T = -(\partial \ln K/\partial \ln V)_P$ is greater than

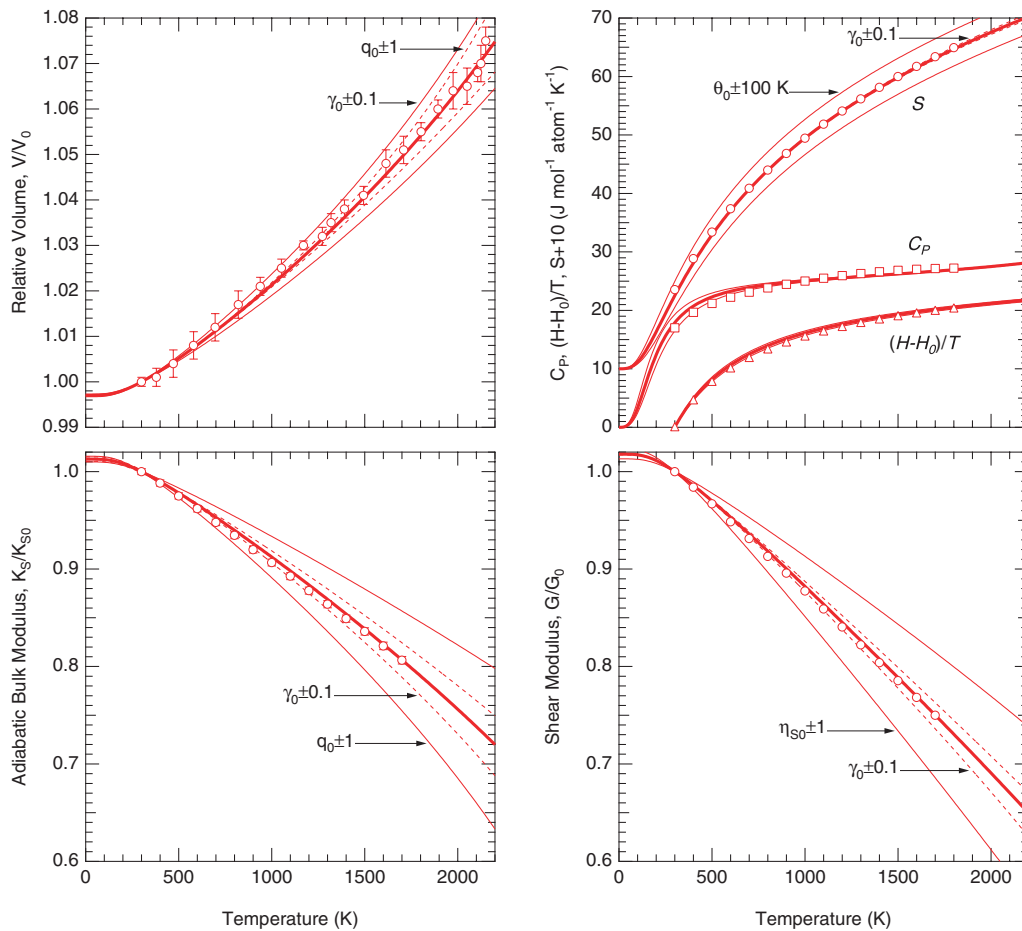


Figure 7. Experimental determinations of thermal expansion (Bouhifd *et al.* 1996), thermochemical quantities (Robie & Hemingway 1995), adiabatic bulk modulus and shear modulus (Anderson & Isaak 1995) of forsterite compared with the thermodynamic model described in the text for (bold lines) values of parameters from Table A1 and (thin solid and dashed lines) for deviations from these values as shown. The entropy is shifted upwards for clarity.

$K' = -(\partial \ln K / \partial \ln V)_T$. The ability to compare the relative magnitude of temperature and pressure derivatives in this way is one advantage of using δ_G as we have defined it here, rather than the alternative quantity $\Gamma \equiv -(\partial G / \partial T)_P (\alpha G)^{-1}$, which is not as simply related to G' .

6 APPLICATIONS

The shear wave velocity of mantle phases and its variation with temperature and composition form a foundation for interpretation of seismological observations in terms of the thermal and chemical state of the mantle. We present estimates of each of these quantities for each of the major mantle phases. Because this paper focuses on physical properties rather than phase equilibria and for the purposes of illustration, we have simplified the chemical compositions of the phases as they would exist in the mantle. We have assumed that each phase has constant composition with depth and we have considered only the most abundant end-members. Phases with Mg-Fe solid solution are assumed to have $X_{\text{Fe}} = 0.1$. We neglect the Al content of all phases except for garnet. We neglect the Ca content of garnet and majorite. We draw separate curves for garnet (py-al solid solution) and majorite (Al-free Mg-Fe metasilicate composition) to illustrate the influence of the depth-dependent change in composition that the garnet–majorite phase undergoes as it dissolves the pyroxenes. Uncertainties are formally propagated from those shown in Table A1.

In the upper mantle and transition zone, we find that the change in shear wave velocity as a result of phase transformations exceeds the influence of pressure on the velocity of any one phase (Fig. 9). This confirms the essential role that phase transformations play in producing the anomalous velocity gradient of the transition zone. Comparison to seismological observations confirms the standard model of a homogeneous peridotite-like composition that produces a series of phase transformations with increasing depth: the velocity of the upper mantle is spanned by that of olivine, opx and cpx, and garnet, in the shallow transition zone (410–520 km) by cpx, majorite and wadsleyite, and in the deep transition zone (500–660 km) by Ca-perovskite, ringwoodite and majorite. Velocity in the lower mantle is spanned by those of Mg-perovskite, magnesiowüstite and Ca-perovskite. Ca-perovskite is the fastest major mineral in the lower mantle; its velocity is exceeded over part of the lower mantle only by stishovite (not shown), a minor phase that is not expected to be present globally. We caution that the first principles calculations upon which our Ca-perovskite results are based on a cubic ground state structure, an assumption not supported by other

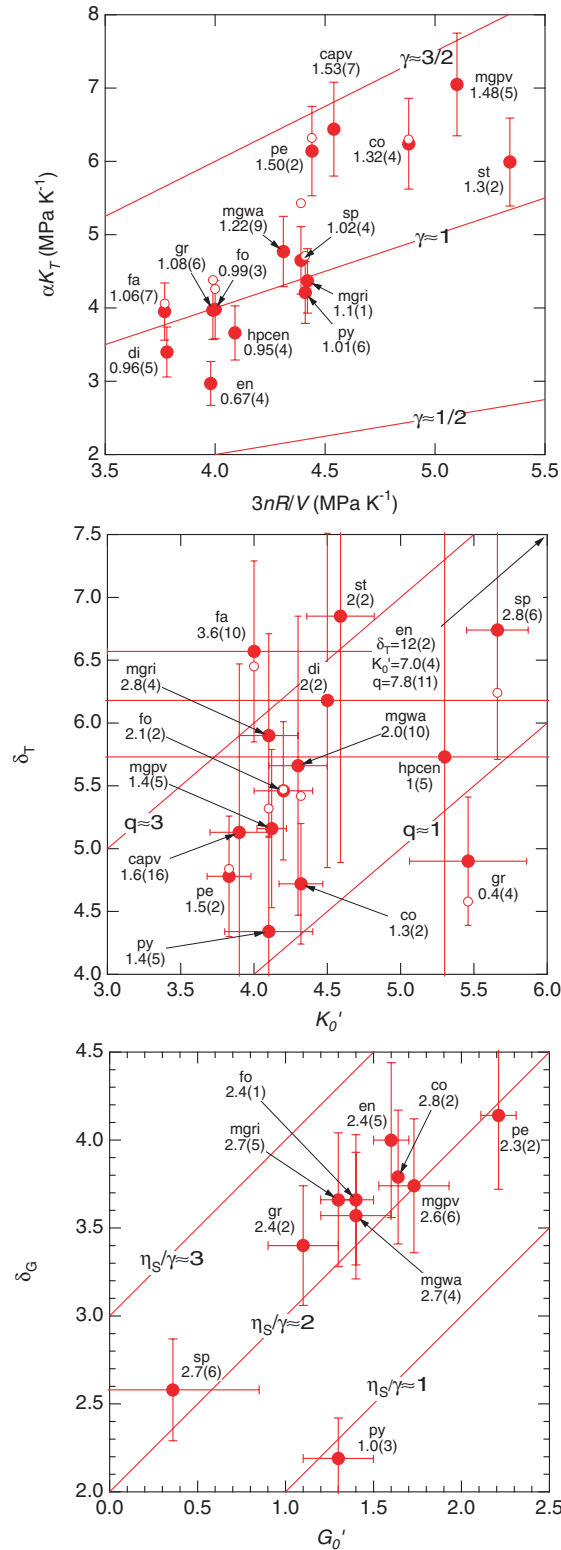


Figure 8. (Symbols) Experimental data compared with (lines) expected parameter values for (top) $\gamma = \alpha K_T / C_V V^{-1}$ (middle) $q \approx \delta_T - K'_0 + 1$ and (bottom) $\eta_S / \gamma \approx \delta_G - G'_0$ as described in the text. For each symbol, the species and our preferred parameter value from Table A1 are indicated. Open symbols are values given by Anderson & Isaak (1995) at 1000 K or at the highest temperature reported if this is less than 1000 K. Solid symbols with error bars are our own summary of experimental data as follows: αK_T estimated as $\langle \alpha \rangle K_T(\langle T \rangle)$ where $\langle \alpha \rangle$ is the average value of α over a range of temperature from room temperature to 1000 K or the maximum temperature reported, with midpoint ($\langle T \rangle$) and K_T from either P - V - T equation of state data or ultrasonic data in which case the appropriate adiabatic to isothermal correction is performed. δ_T from P - V - T equation of state studies or from ultrasonic data in which case we apply the correction $\delta_T \approx \delta_S + \gamma$, where γ is from Table A1. δ_G from ultrasonic measurements of $G(T)$. Error bars based on a nominal uncertainty of 10 per cent in αK_T , and reported uncertainties in dK/dT and dG/dT .

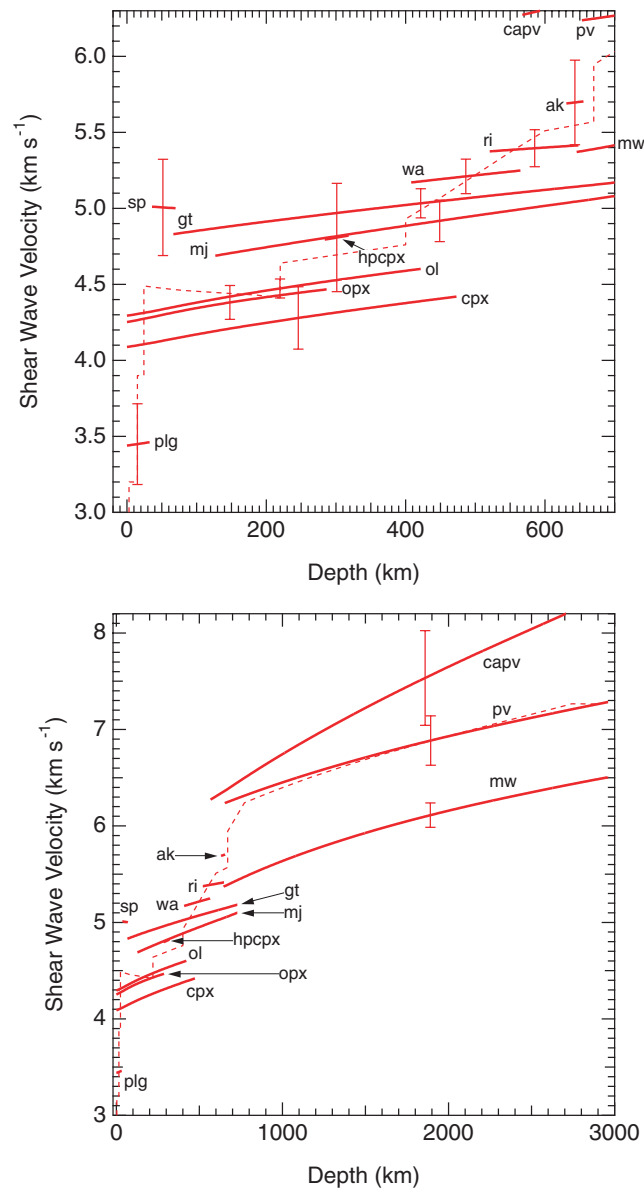


Figure 9. Shear wave velocities calculated according to our theory and the parameters in Table A1 along a typical geotherm for (bottom) the whole mantle and (top) an expanded depth scale to show details of the upper mantle. Uncertainties are propagated from parameter uncertainties shown in Table A1. We show (dashed) the shear wave velocity in PREM (Dziewonski & Anderson 1981) for comparison. Phases are shown over the approximate depth range that they are expected to occur in the mantle. Solid solutions are assumed to consist of Mg and Fe end-members with $X_{\text{Fe}} = 0.1$. Garnet ($0.9\text{py} + 0.1\text{al}$) and majorite ($\text{mgmj} + 2/15\text{al} - 2/15\text{py}$) components are shown separately to emphasize the large variations in composition with depth expected for the garnet–majorite phase. The geotherm along which the calculations are performed is the adiabatic portion of that given by Stacey (1992); we have removed the thermal boundary layers by extending the adiabatic portion smoothly to the surface (1573 K) and to the core–mantle boundary (3015 K).

theoretical calculations (Stixrude *et al.* 1996; Akber-Knutson *et al.* 2002; Magyari-Kope *et al.* 2002) or experiment (Shim *et al.* 2002; Ono *et al.* 2004). Knowledge of the shear wave velocity of Ca-perovskite is essential for evaluating the seismic visibility of Ca as a chemical component in the lower mantle, and its potential influence on radial and lateral structure (Karato & Karki 2001).

One of the most remarkable patterns in the temperature and compositional derivatives is the large difference between garnet–majorite and other phases (Fig. 10). The compositional derivative for garnet and majorite (and cpx) is only a third that of olivine and opx, while the temperature derivatives of garnet and majorite are approximately half that of olivine and opx. The contrast in compositional derivatives can be traced directly to the shear modulus of Mg and Fe end-members of the phases: while the shear modulus of fayalite is 40 per cent less than that of forsterite, that of almandine is actually slightly greater than that of pyrope, partially offsetting the effect of the greater density of almandine on V_S . The contrast in temperature derivatives can be related to experimental measurements of dG/dT of the dominant species: 8 and 9 MPa K⁻¹ for pyrope and majorite, respectively, compared with 15 MPa K⁻¹ for forsterite (Anderson & Isaak 1995; Sinogeikin & Bass 2002b). One consequence of the unusual properties of garnet is that the influence of temperature and iron content will be very sensitive to bulk composition. More garnet-rich compositions, such as basalt, will be much less sensitive to variations in temperature or iron content than

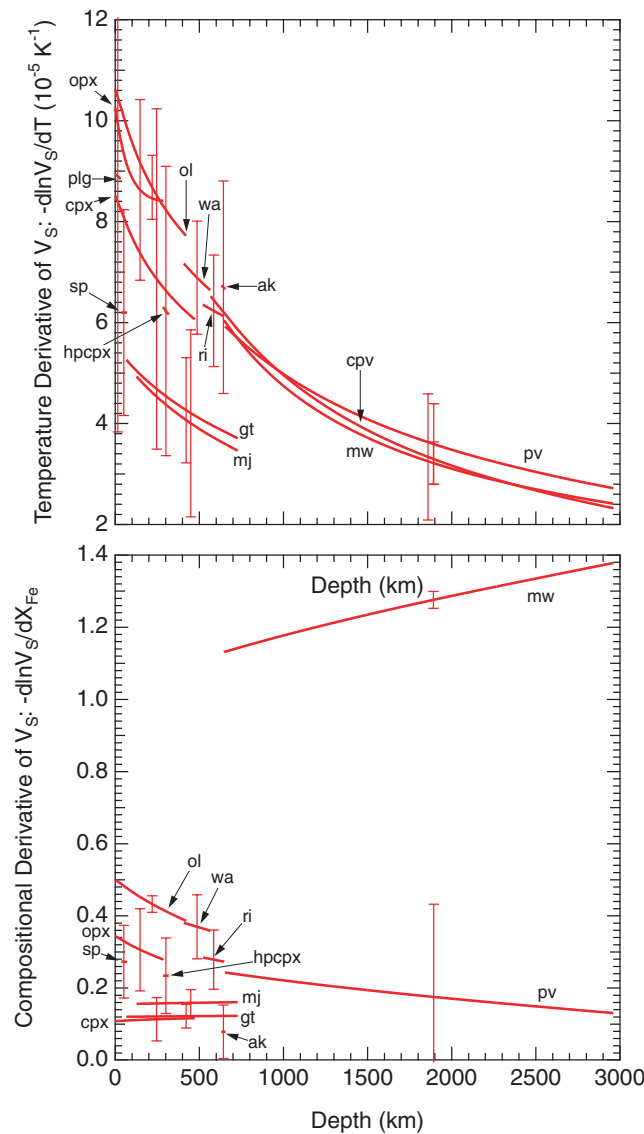


Figure 10. Variation of the shear wave velocity with respect to (top) temperature and (bottom) composition calculated from our theory and parameters of Table A1. Uncertainties are propagated from parameter uncertainties shown in Table A1.

garnet-poor bulk compositions such as harzburgite. The dependence of the shear modulus of garnet on composition has been discussed in terms of the unique coordination state of Mg/Fe in garnet (eightfold) as compared with most other mantle minerals (sixfold) (Jackson *et al.* 1978; Leitner *et al.* 1980).

7 CONCLUSIONS

When Davies (1974) developed the quasi-harmonic theory of the elastic moduli, little was known experimentally of the properties of mantle minerals at elevated pressure or temperature. The rapid growth in our knowledge in the intervening years has now made it possible for the first time to test many of the assumptions made by Davies (1974), and in the foundational studies of Leibfried & Ludwig (1961) and Thomsen (1972). In particular, the Eulerian finite strain description of the cold contribution, known for some time now to be unsurpassed as a description of the equation of state, appears to perform equally well in the case of the elastic moduli, although reliable results at compressions sufficiently large for definitive tests are still few. Thermal properties revolve around the Grüneisen parameter, γ , the volume dependence of which has been the topic of speculation for decades. The Eulerian finite strain expansion for the vibrational frequencies appears to be able to reproduce the proper behaviour of γ with a minimum of free parameters. The Grüneisen parameter is properly a second-rank and its strain derivative η_{ijkl} a fourth-rank tensor. Experimental data are currently on the verge of being able to resolve the anisotropy of these two tensors.

Another important property of the theory of Davies (1974) is that it is readily incorporated within the framework of a fundamental thermodynamic relation. Not only the elastic moduli, but all other thermodynamic properties, including the Gibbs free energy and phase equilibria, may be computed from a single functional form. We have illustrated here the scope of our theory as applied to physical properties and will illustrate further applications to phase equilibria in Paper II.

A thermodynamically self-consistent theory of the kind we have presented is an important complement to experimental measurement and first principles theory. Extrapolation and interpolation will always be an essential part of our understanding of the mantle because the range of pressure, temperature and composition is so vast. Perhaps more importantly, a semi-empirical thermodynamic theory provides a formal framework in which to view intensive studies of individual phases and species. We have sought to illustrate this aspect of the theory via an interim synthesis of available information.

ACKNOWLEDGMENTS

We are grateful to Ian Jackson and an anonymous referee for their constructive reviews. We thank M. Bukowinski and R. Jeanloz for insightful comments. This work was partly supported by the CSEDI programme of the National Science Foundation under grant EAR-0079980, and by fellowships from the David and Lucile Packard and the Alfred P. Sloan foundations awarded to CLB. We are also thankful for the sponsorship and support of the MarMar Institute.

REFERENCES

- Agnon, A. & Bukowinski, M.S.T., 1990. Thermodynamic and elastic properties of a many-body model for simple oxides, *Phys. Rev. B*, **41**(11), 7755–7766.
- Akber-Knutson, S., Bukowinski, M.S.T. & Matas, J., 2002. On the structure and compressibility of CaSiO₃ perovskite, *Geophys. Res. Lett.*, **29**(3), 1034, doi:10.1029/2001GL013523.
- Anderson, D.L., 1987. Thermally induced phase changes, lateral heterogeneity of the mantle, continental roots, and deep slab anomalies, *J. geophys. Res.*, **92**, 13 968–13 980.
- Anderson, O.L., 1995. *Equations of State of Solids for Geophysics and Ceramic Science*, Oxford University Press, Oxford.
- Anderson, O.L. & Isaak, D.G., 1995. Elastic constants of mantle minerals at high temperature, in *Mineral Physics and Crystallography: A Handbook of Physical Constants*, pp. 64–97, ed. Ahrens, T.J., American Geophysical Union, Washington, DC.
- Anderson, O.L., Schreiber, E. & Lieberman, R.C., 1968. Some elastic constant data on minerals relevant to geophysics, *Rev. Geophys.*, **6**(4), 491–524.
- Andraut, D., Angel, R.J., Mosenfelder, J.L. & Bihan, T.L., 2003. Equation of state of stishovite to lower mantle pressures, *Am. Mineral.*, **88**(2–3), 301–307.
- Angel, R.J., Hazen, R.M., McCormick, T.C., Prewitt, C.T. & Smyth, J.R., 1988. Comparative compressibility of end-member feldspars, *Phys. Chem. Miner.*, **15**(4), 313–318.
- Anovitz, L.M., Essene, E.J., Metz, G.W., Bohlen, S.R., Westrum, E.F. & Hemingway, B.S., 1993. Heat-capacity and phase-equilibria of almandine, Fe₃Al₂Si₃O₁₂, *Geochim. cosmochim. Acta.*, **57**(17), 4191–4204.
- Barron, T.H.K., Berg, W.T. & Morrison, J.A., 1957. The thermal properties of alkali halide crystals .2. analysis of experimental results, *Proc. R. Soc. Lon. Ser.-A.*, **242**(1231), 478–492.
- Bass, J.D., 1995. Elasticity of minerals, glasses, and melts, in *Mineral Physics and Crystallography: A Handbook of Physical Constants*, pp. 45–63, ed. Ahrens, T.J., American Geophysical Union, Washington, DC.
- Bass, J.D., Liebermann, R.C., Weidner, D.J. & Finch, S.J., 1981. Elastic properties from acoustic and volume compression experiments, *Phys. Earth planet. Int.*, **25**(2), 140–158.
- Berman, R.G., 1988. Internally-consistent thermodynamic data for minerals in the system Na₂O-K₂O-CaO-MgO-FeO-Fe₂O₃-Al₂O₃-SiO₂-TiO₂-H₂O-CO₂, *J. Petrol.*, **29**(2), 445–522.
- Birch, F., 1952. Elasticity and constitution of the earth's interior, *J. geophys. Res.*, **57**, 227–286.
- Boehler, R. & Ramakrishnan, J., 1980. Experimental results on the pressure-dependence of the gruneisen-parameter—a review, *J. geophys. Res.*, **85**(NB12), 6996–7002.
- Bouhifd, M.A., Andraut, D., Fiquet, G. & Richet, P., 1996. Thermal expansion of forsterite up to the melting point, *Geophys. Res. Lett.*, **23**(10), 1143–1146.
- Callen, H.B., 1960. *Thermodynamics*, John Wiley and Sons, New York.
- Cammarano, F., Goes, S., Vacher, P. & Giardini, D., 2003. Inferring upper-mantle temperatures from seismic velocities, *Phys. Earth planet. Int.*, **138**(3–4), 197–222.
- Carter, W.J., Marsh, S.P., Fritz, N.J. & McQueen, R.G., 1971. The equation of state of selected materials for high pressure reference, in *Accurate characterization of the high pressure environment*, Vol. 326, pp. 147–158, ed. Lloyd, E.C., NBS Special Publications, National Bureau of Standards, Washington.
- Chaplot, S.L., Choudhury, N., Ghose, S., Rao, M.N., Mittal, R. & Goel, P., 2002. Inelastic neutron scattering and lattice dynamics of minerals, *Eur. J. Mineral.*, **14**(2), 291–329.
- Chopelas, A., 1999. Estimates of mantle relevant clapeyron slopes in the MgSiO₃ system from high-pressure spectroscopic data, *Am. Mineral.*, **84**(3), 233–244.
- Conrad, P.G., Zha, C.S., Mao, H.K. & Hemley, R.J., 1999. The high-pressure, single-crystal elasticity of pyrope, grossular, and andradite, *Am. Mineral.*, **84**(3), 374–383.
- Dasilva, C.R.S., Karki, B.B., Stixrude, L. & Wentzcovitch, R.M., 1999. Ab initio study of the elastic behavior of MgSiO₃ ilmenite at high pressure, *Geophys. Res. Lett.*, **26**(7), 943–946.
- Davies, G.F., 1974. Effective elastic-moduli under hydrostatic stress. I. quasi-harmonic theory, *J. Phys. Chem. Solids*, **35**(11), 1513–1520.
- Davies, G.F. & Dziewonski, A.M., 1975. Homogeneity and constitution of earth's lower mantle and outer core, *Phys. Earth planet. Int.*, **10**(4), 336–343.
- Duffy, T.S. & Anderson, D.L., 1989. Seismic velocities in mantle minerals and the mineralogy of the upper mantle, *J. Geophys. Res.-Solid*, **94**(B2), 1895–1912.
- Dziewonski, A.M. & Anderson, D.L., 1981. Preliminary reference earth model, *Phys. Earth planet. Int.*, **25**, 297–356.
- Fei, Y., 1995. Thermal expansion, in *Mineral Physics and Crystallography: A Handbook of Physical Constants*, pp. 29–44, ed. Ahrens, T.J., American Geophysical Union, Washington, DC.
- Fei, Y.W. & Saxena, S.K., 1990. Internally consistent thermodynamic data and equilibrium phase-relations for compounds in the system mgo-sio₂ at high-pressure and high-temperature, *J. Geophys. Res.-Solid*, **95**(B5), 6915–6928.
- Fei, Y.W., Mao, H.K., Shu, J.F., Parthasarathy, G., Bassett, W.A. & Ko, J.D., 1992. Simultaneous high-p, high-t X-Ray-Diffraction study of Beta-(Mg, Fe)₂SiO₄ to 26-gpa and 900-k, *J. Geophys. Res.-Sol. Ea.*, **97**(B4), 4489–4495.
- Fiquet, G., Richet, P. & Montagnac, G., 1999. High-temperature thermal expansion of lime, periclase, corundum and spinel, *Phys. Chem. Miner.*, **27**(2), 103–111.
- Fiquet, G., Dewaele, A., Andraut, D., Kunz, M. & Bihan, T.L., 2000. Thermoelastic properties and crystal structure of MgSiO₃ perovskite at lower mantle pressure and temperature conditions, *Geophys. Res. Lett.*, **27**, 21–24.
- Flesch, L.M., Li, B.S. & Liebermann, R.C., 1998. Sound velocities of polycrystalline MgSiO₃-orthopyroxene to 10 GPa at room temperature, *Am. Mineral.*, **83**(5–6), 444–450.
- Frisillo, A.L. & Barsch, G.R., 1972. Measurement of single-crystal elastic-constants of bronzite as a function of pressure and temperature, *J. geophys. Res.*, **77**(32), 6360–6384.
- Ghiorso, M.S. & Sack, R.O., 1995. Chemical mass-transfer in magmatic processes. 4. A revised and internally consistent thermodynamic model

- for the interpolation and extrapolation of liquid-solid equilibria in magmatic systems at elevated-temperatures and pressures, *Contrib. Mineral. Petr.*, **119**(2–3), 197–212.
- Gieske, J.H. & Barsch, G.R., 1968. Pressure dependence of elastic constants of single crystalline aluminum oxide, *Phys. Status Solidi*, **29**(1), 121–131.
- Hacker, B.R., Abers, G.A. & Peacock, S.M., 2003. Subduction factory—1. theoretical mineralogy, densities, seismic wave speeds, and H₂O contents, *J. Geophys. Res.-Sol. Ea.*, **108**(B1), B012029, doi:10.1029/2001JB001127.
- Harrison, R.J., Redfern, S.A.T. & O'Neill, H.S.C., 1998. The temperature dependence of the cation distribution in synthetic hercynite (FeAl₂O₄) from in-situ neutron structure refinements, *Am. Mineral.*, **83**(9–10), 1092–1099.
- Haselton, H.T., Robie, R.A. & Hemingway, B.S., 1987. Heat-capacities of synthetic hedenbergite, ferrobustamite, and CaFeSi₂O₆ glass, *Geochim. cosmochim. Acta.*, **51**(8), 2211–2217.
- Holland, T.J.B. & Powell, R., 1990. An enlarged and updated internally consistent thermodynamic dataset with uncertainties and correlations—the system K₂O-Na₂O-CaO-MgO-MnO-FeO-Fe₂O₃-Al₂O₃-TiO₂-SiO₂-C-H₂O₂, *J. Metamorph. Geol.*, **8**(1), 89–124.
- Holland, T.J.B. & Powell, R., 1998. An internally consistent thermodynamic data set for phases of petrological interest, *J. Metamorph. Geol.*, **16**(3), 309–343.
- Hugh-Jones, D.A., 1997. Thermal expansion of MgSiO₃ and FeSiO₃ ortho- and clinopyroxenes, *Am. Mineral.*, **82**(7–8), 689–696.
- Hugh-Jones, D.A. & Angel, R.J., 1997. Effect of Ca²⁺ and Fe²⁺ on the equation of state of MgSiO₃ orthopyroxene, *J. Geophys. Res.-Sol. Ea.*, **102**(B6), 12 333–12 340.
- Hugh-Jones, D.A., Sharp, T., Angel, R. & Woodland, A., 1996. The transition of orthoferrosilite to high-pressure C₂/c clinoferrosilite at ambient temperature, *Eur. J. Mineral.*, **8**(6), 1337–1345.
- Ita, J. & Stixrude, L., 1992. Petrology, elasticity, and composition of the mantle transition zone, *J. Geophys. Res.-Sol. Ea.*, **97**(B5), 6849–6866.
- Jackson, I. & Rigden, S.M., 1996. Analysis of P-V-T data; constraints on the thermoelastic properties of high-pressure minerals, *Phys. Earth planet. Int.*, **96**, 85–112.
- Jackson, I., Liebermann, R.C. & Ringwood, A.E., 1978. Elastic properties of (Mg_xFe_{1-x})O solid-solutions, *Phys. Chem. Miner.*, **3**(1), 11–31.
- Jackson, I., Khanna, S.K., Revcolevschi, A. & Berthon, J., 1990. Elasticity, shear-mode softening and high-pressure polymorphism of wüstite (Fe_{1-x}O), *J. Geophys. Res.-Solid*, **95**(B13), 21 671–21 685.
- Jackson, J.M., Sinogeikin, S.V. & Bass, J.D., 1999. Elasticity of MgSiO₃ orthoenstatite, *Am. Mineral.*, **84**(4), 677–680.
- Jackson, J.M., Palko, J.W., Andrault, D., Sinogeikin, S.V., Lakshtanov, D.L., Wang, J.Y., Bass, J.D. & Zha, C.S., 2003. Thermal expansion of natural orthoenstatite to 1473 K, *Eur. J. Mineral.*, **15**(3), 469–473.
- Jacobsen, S.D., Reichmann, H.J., Spetzler, H.A., Mackwell, S.J., Smyth, J.R., Angel, R.J. & McCammon, C.A., 2002. Structure and elasticity of single-crystal (Mg,Fe)O and a new method of generating shear waves for gigahertz ultrasonic interferometry, *J. Geophys. Res.-Sol. Ea.*, **107**(B2), B022037, doi:10.1029/2001JB00049D.
- Jeanloz, R., 1989. Shock-wave equation of state and finite strain theory, *J. Geophys. Res.-Solid*, **94**(B5), 5873–5886.
- Jeanloz, R. & Thompson, A.B., 1983. Phase transitions and mantle discontinuities, *Rev. Geophys.*, **21**, 51–74.
- Karato, S. & Karki, B.B., 2001. Origin of lateral variation of seismic wave velocities and density in the deep mantle, *J. Geophys. Res.-Sol. Ea.*, **106**(B10), 21 771–21 783.
- Karki, B.B. & Crain, J., 1998. First-principles determination of elastic properties of CaSiO₃ perovskite at lower mantle pressures, *Geophys. Res. Lett.*, **25**(14), 2741–2744.
- Karki, B.B., Stixrude, L., Clark, S.J., Warren, M.C., Ackland, G.J. & Crain, J., 1997. Elastic properties of orthorhombic MgSiO₃ perovskite at lower mantle pressures, *Am. Mineral.*, **82**, 635–638.
- Karki, B.B., Wentzcovitch, R.M., de Gironcoli, S. & Baroni, S., 2000a. Ab initio lattice dynamics of MgSiO₃ perovskite at high pressure, *Phys. Rev. B*, **62**(22), 14 750–14 756.
- Karki, B.B., Wentzcovitch, R.M., de Gironcoli, S. & Baroni, S., 2000b. High-pressure lattice dynamics and thermoelasticity of MgO, *Phys. Rev. B*, **61**(13), 8793–8800.
- Karki, B.B., Stixrude, L. & Wentzcovitch, R.M., 2001. High-pressure elastic properties of major materials of earth's mantle from first principles, *Rev. Geophys.*, **39**(4), 507–534.
- Katsura, T. *et al.*, 2004. Thermal expansion of Mg₂SiO₄ ringwoodite at high pressures, *J. Geophys. Res.-Sol. Ea.*, **109**(B12), B02209, doi:10.1029/2003JB002438.
- Kiefer, B., Stixrude, L. & Wentzcovitch, R.M., 2002. Elasticity of (Mg, Fe)SiO₃-Perovskite at high pressures, *Geophys. Res. Lett.*, **29**(11), 1539, doi:10.1029/2002GL014683.
- Kieffer, S.W., 1980. Thermodynamics and lattice-vibrations of minerals 4. application to chain and sheet silicates and orthosilicates, *Rev. Geophys.*, **18**, 862–886.
- Knittle, E., 1995. Static compression measurements of equations of state, in *Mineral Physics and Crystallography: A Handbook of Physical Constants*, pp. 98–142, ed. Ahrens, T.J., American Geophysical Union, Washington, DC.
- Krupka, K.M., Robie, R.A., Hemingway, B.S., Kerrick, D.M. & Ito, J., 1985. Low-temperature heat-capacities and derived thermodynamic properties of anthophyllite, diopside, enstatite, bronzite, and wollastonite, *Am. Mineral.*, **70**(3–4), 249–260.
- Kubo, A. & Akaogi, M., 2000. Post-garnet transitions in the system Mg₄Si₄O₁₂-Mg₃Al₂Si₃O₁₂ up to 28 GPa: phase relations of garnet, ilmenite and perovskite, *Phys. Earth planet. Int.*, **121**(1–2), 85–102.
- Kuskov, O.L., 1995. Constitution of the Moon: 3. Composition of middle mantle from seismic data, *Phys. Earth. Planet. Inter.*, **90**(1–2), 55–74.
- Leibfried, G. & Ludwig, W., 1961. Theory of anharmonic effects in crystals, *Solid State Phys.*, **12**, 275–444.
- Leitner, B.J., Weidner, D.J. & Liebermann, R.C., 1980. Elasticity of single-crystal pyrope and implications for garnet solid-solution series, *Phys. Earth planet. Int.*, **22**(2), 111–121.
- Levien, L. & Prewitt, C.T., 1981. High-pressure structural study of diopside, *Am. Mineral.*, **66**(3–4), 315–323.
- Li, B.S., Liebermann, R.C. & Weidner, D.J., 2001. P-V-Vp-Vs-T measurements on wadsleyite to 7 GPa and 873 K: implications for the 410-km seismic discontinuity, *J. Geophys. Res.-Sol. Ea.*, **106**(B12), 30 579–30 591.
- Liu, J., Zhang, J.Z., Flesch, L., Li, B.S., Weidner, D.J. & Liebermann, R.C., 1999. Thermal equation of state of stishovite, *Phys. Earth planet. Int.*, **112**(3–4), 257–266.
- Luo, S.N., Mosenfelder, J.L., Asimow, P.D. & Ahrens, T.J., 2002. Direct shock wave loading of stishovite to 235 GPa: implications for perovskite stability relative to an oxide assemblage at lower mantle conditions, *Geophys. Res. Lett.*, **29**(14), 1691, doi:10.1029/2002GL015627.
- Magyari-Kope, B., Vitos, L., Grimvall, G., Johansson, B. & Kollar, J., 2002. Low-temperature crystal structure of CaSiO₃ perovskite: An ab initio total energy study, *Phys. Rev. B*, **65**(19), 193107.
- Mao, H.K., Takahashi, T., Bassett, W.A. & Weaver, J.S., 1969. Effect of pressure and temperature on molar volumes of wüstite and of 3 (Fe Mg)₂SiO₄ spinel solid solutions, *J. geophys. Res.*, **74**(4), 1061–1069.
- Marton, F.C. & Cohen, R.E., 2002. Constraints on lower mantle composition from molecular dynamics simulations of MgSiO₃ perovskite, *Phys. Earth Planet. Int.*, **134**(3–4), 239–252.
- Mattern, E., Matas, J., Ricard, Y. & Bass, J., 2005. Lower mantle composition and temperature from mineral physics and thermodynamic modelling, *Geophys. J. Int.*, **160**, 973–990.
- Nye, J.F., 1985. *Physical Properties of Crystals: Their Representation by Tensors and Matrices*, 2nd edn, Oxford University Press, Oxford.
- Oganov, A.R. & Dorogokupets, P.I., 2003. All-electron and pseudopotential study of MgO: equation of state, anharmonicity, and stability, *Phys. Rev. B*, **67**(22), 224110.
- Oganov, A.R., Brodholt, J.P. & Price, G.D., 2001a. Ab initio elasticity and thermal equation of state of MgSiO₃ perovskite, *Earth planet. Sci. Lett.*, **184**, 555–560.
- Oganov, A.R., Brodholt, J.P. & Price, G.D., 2001b. The elastic constants of MgSiO₃ perovskite at pressures and temperatures of the earth's mantle, *Nature*, **411**(6840), 934–937.

- Oneill, B., Bass, J.D., Smyth, J.R. & Vaughan, M.T., 1989. Elasticity of a grossular-pyrope-almandine garnet, *J. Geophys. Res.-Solid*, **94**(B12), 17 819–17 824.
- Ono, S., Ohishi, Y. & Mibe, K., 2004. Phase transition of Ca-perovskite and stability of Al-bearing Mg-perovskite in the lower mantle, *Am. Mineral.*, **89**(10), 1480–1485.
- Robie, R.A. & Hemingway, B.S., 1995. Thermodynamic Properties of Minerals and Related Substances at 298.15 K and 1 Bar (10^5 Pascals) Pressure and at Higher Temperature, *US Geological Survey Bulletin*, **2131**, 461.
- Robie, R.A., Hemingway, B.S. & Takei, H., 1982. Heat-capacities and entropies of Mg_2SiO_4 , Mn_2SiO_4 , and Co_2SiO_4 between 5-k and 380-k, *Am. Mineral.*, **67**(5–6), 470–482.
- Sammis, C., Anderson, D. & Jordan, T., 1970. Application of isotropic finite strain theory to ultrasonic and seismological data, *J. Geophys. Res.*, **75**(23), 4478–4480.
- Shim, S.H. & Duffy, T.S., 2000. Constraints on the P-V-T equation of state of MgSiO_3 perovskite, *Am. Mineral.*, **85**(2), 354–363.
- Shim, S.H., Duffy, T.S. & Shen, G.Y., 2000. The stability and P-V-T equation of state of CaSiO_3 perovskite in the earth's lower mantle, *J. Geophys. Res.-Sol. Ea.*, **105**(B11), 25 955–25 968.
- Shim, S.H., Duffy, T.S. & Kenichi, T., 2002. Equation of state of gold and its application to the phase boundaries near 660 km depth in earth's mantle, *Earth planet. Sci. Lett.*, **203**(2), 729–739.
- Shinmei, T., Tomioka, N., Fujino, K., Kuroda, K. & Irifune, T., 1999. In situ X-ray diffraction study of enstatite up to 12 GPa and 1473 K and equations of state, *Am. Mineral.*, **84**(10), 1588–1594.
- Sinogeikin, S.V. & Bass, J.D., 2000. Single-crystal elasticity of pyrope and MgO to 20 GPa by Brillouin scattering in the diamond cell, *Phys. Earth planet. Int.*, **120**(1–2), 43–62.
- Sinogeikin, S.V. & Bass, J.D., 2002a. Elasticity of majorite and a majorite-pyrope solid solution to high pressure: Implications for the transition zone, *Geophys. Res. Lett.*, **29**(2), 1017, doi:10.1029/2001GL013937.
- Sinogeikin, S.V. & Bass, J.D., 2002b. Elasticity of pyrope and majorite-pyrope solid solutions to high temperatures, *Earth planet. Sci. Lett.*, **203**(1), 549–555.
- Sinogeikin, S.V., Bass, J.D., Kavner, A. & Jeanloz, R., 1997. Elasticity of natural majorite and ringwoodite from the catherwood meteorite, *Geophys. Res. Lett.*, **24**(24), 3265–3268.
- Sinogeikin, S.V., Katsura, T. & Bass, J.D., 1998. Sound velocities and elastic properties of Fe-bearing wadsleyite and ringwoodite, *J. Geophys. Res.-Sol. Ea.*, **103**(B9), 20 819–20 825.
- Sinogeikin, S.V., Bass, J.D. & Katsura, T., 2001. Single-crystal elasticity of $\gamma\text{-}(\text{Mg}_{0.9}\text{Fe}_{0.09})_2\text{SiO}_4$ to high pressures and to high temperatures, *Geophys. Res. Lett.*, **28**(22), 4335–4338.
- Sinogeikin, S.V., Zhang, J.Z. & Bass, J.D., 2004. Elasticity of single crystal and polycrystalline MgSiO_3 perovskite by Brillouin spectroscopy, *Geophys. Res. Lett.*, **31**(6), L06620, doi:10.1029/2004GL019559.
- Skinner, B.J. & Boyd, F.R., 1964. Aluminous enstatites, *Carnegie I. Wash.*, **63**, 163–165.
- Smyth, J.R. & McCormick, T.C., 1995. Crystallographic data for minerals, in *Mineral Physics and Crystallography: A Handbook of Physical Constants*, pp. 1–17, ed. Ahrens, T.J., American Geophysical Union, Washington, DC.
- Sobolev, S.V. & Babeyko, A.Y., 1994. Modeling of mineralogical composition, density and elastic-wave velocities in anhydrous magmatic rocks, *Surv. Geophys.*, **15**(5), 515–544.
- Speziale, S., Zha, C.S., Duffy, T.S., Hemley, R.J. & Mao, H.K., 2001. Quasi-hydrostatic compression of magnesium oxide to 52 GPa: implications for the pressure-volume-temperature equation of state, *J. Geophys. Res.-Sol. Ea.*, **106**(B1), 515–528.
- Stacey, F.D., 1992. *Physics of the Earth*, 3rd edn, Brookfield, Brisbane.
- Stixrude, L. & Bukowinski, M.S.T., 1990. Fundamental thermodynamic relations and silicate melting with implications for the constitution of D'' , *J. Geophys. Res.*, **95**, 19 311–19 325.
- Stixrude, L. & Bukowinski, M.S.T., 1993. Thermodynamic analysis of the system MgO-FeO-SiO_2 at high pressure and the structure of the lowermost mantle, in *Evolution of the earth and planets*, pp. 131–142, eds Takahashi, E., Jeanloz, R. & Rubie, D., International Union of Geodesy and Geophysics, Washington, DC.
- Stixrude, L. & Lithgow-Bertelloni, C., 2005. Mineralogy and elasticity of the oceanic upper mantle: Origin of the low-velocity zone, *J. Geophys. Res.*, **110**(B3), B03204.
- Stixrude, L., Hemley, R.J., Fei, Y. & Mao, H.K., 1992. Thermoelasticity of silicate perovskite and magnesio-wüstite and stratification of the earth's mantle, *Science*, **257**, 1099–1101.
- Stixrude, L., Cohen, R.E., Yu, R.C. & Krakauer, H., 1996. Prediction of phase transition in CaSiO_3 perovskite and implications for lower mantle structure, *Am. Mineral.*, **81**, 1293–1296.
- Stolen, S., Glockner, R., Gronvold, F., Atake, T. & Izumisawa, S., 1996. Heat capacity and thermodynamic properties of nearly stoichiometric wüstite from 13 to 450 K, *Am. Mineral.*, **81**(7–8), 973–981.
- Thieblot, L., Roux, J. & Richet, P., 1998. High-temperature thermal expansion and decomposition of garnets, *Eur. J. Mineral.*, **10**(1), 7–15.
- Thieblot, L., Tequi, C. & Richet, P., 1999. High-temperature heat capacity of grossular ($\text{Ca}_3\text{Al}_2\text{Si}_3\text{O}_{12}$), enstatite (MgSiO_3), and titanite (CaTiSiO_5), *Am. Mineral.*, **84**(5–6), 848–855.
- Thompson, K.T., Wentzcovitch, R.M. & Bukowinski, M.S.T., 1996. Polymorphs of alumina predicted by first principles: Putting pressure on the ruby scale, *Science*, **274**, 1880–1882.
- Thomsen, L., 1972. Fourth-order anharmonic theory—elasticity and stability, *J. Phys. Chem. Solids*, **33**(2), 363–378.
- Thurston, R.N., 1965. Effective elastic coefficients for wave propagation in crystals under stress, *J. Acoust. Soc. Am.*, **37**(2), 348–356.
- Tribaudino, M., Principe, M., Nestola, F. & Hanfland, M., 2001. A $\text{P}_{21/c}$ - $\text{C}_{2/c}$ high-pressure phase transition in $\text{Ca}_{0.5}\text{Mg}_{1.5}\text{Si}_2\text{O}_6$ clinopyroxene, *Am. Mineral.*, **86**(7–8), 807–813.
- Wallace, D.C., 1972. *Thermodynamics of Crystals*, 1st edn, John Wiley and Sons, New York.
- Wang, Y., Weidner, D.J. & Guyot, F., 1996. Thermal equation of state of CaSiO (sub 3) perovskite, *J. Geophys. Res.*, **101**, 661–672.
- Watanabe, H., 1982. Thermochemical properties of synthetic high-pressure compounds relevant to the earth's mantle, in *High-Pressure Research in Geophysics*, pp. 441–464, eds Akimoto, S. & Manghni, M.H., Center for Academic Publications, Tokyo.
- Watt, J.P., Davies, G.F. & Connell, R.J.O., 1976. The elastic properties of composite materials, *Rev. Geophys. Space Phys.*, **14**, 541–563.
- Webb, S.L. & Jackson, I., 1993. The pressure-dependence of the elastic moduli of single-crystal ortho-pyroxene ($\text{Mg}_{0.8}\text{Fe}_{0.2}\text{SiO}_3$), *Eur. J. Mineral.*, **5**(6), 1111–1119.
- Weidner, D.J., 1985. A mineral physics test of a pyrolite mantle, *Geophys. Res. Lett.*, **12**(7), 417–420.
- Weidner, D.J., Bass, J.D., Ringwood, A.E. & Sinclair, W., 1982. The single-crystal elastic moduli of stishovite, *J. Geophys. Res.*, **87**, 4740–4746.
- Wentzcovitch, R.M., Karki, B.B., Cococcioni, M. & de Gironcoli, S., 2004. Thermoelastic properties of MgSiO_3 -perovskite: insights on the nature of the earth's lower mantle, *Phys. Rev. Lett.*, **92**(1), 018501.
- Yoneda, A., 1990. Pressure derivatives of elastic-constants of single-crystal MgO and MgAl_2O_4 , *J. Phys. Earth*, **38**(1), 19–55.
- Zha, C.S., Duffy, T.S., Downs, R.T., Mao, H.K. & Hemley, R.J., 1996. Sound velocity and elasticity of single-crystal forsterite to 16 GPa, *J. Geophys. Res.-Sol. Ea.*, **101**(B8), 17 535–17 545.
- Zha, C.S., Duffy, T.S., Mao, H.K., Downs, R.T., Hemley, R.J. & Weidner, D.J., 1997. Single-crystal elasticity of $\beta\text{-Mg}_2\text{SiO}_4$ to the pressure of the 410 km seismic discontinuity in the earth's mantle, *Earth planet. Sci. Lett.*, **147**, E9–E15.
- Zha, C.S., Duffy, T.S., Downs, R.T., Mao, H.K. & Hemley, R.J., 1998. Brillouin scattering and X-ray diffraction of san carlos olivine: direct pressure determination to 32 GPa, *Earth planet. Sci. Lett.*, **159**(1–2), 25–33.
- Zhang, L., Ahsbahs, H., Kutoglu, A. & Geiger, C.A., 1999. Single-crystal hydrostatic compression of synthetic pyrope, almandine, spessartine, grossular and andradite garnets at high pressures, *Phys. Chem. Miner.*, **27**(1), 52–58.
- Zhao, Y., Dreele, R.B.V., Zhang, J. & Weidner, D.J., 1998. Thermoelastic equation of state of monoclinic pyroxene: $\text{CaMgSi}_2\text{O}_6$, *Rev. High. Press. Sci. Tech.*, **7**, 25–27.
- Zhao, Y.S., Schiferl, D. & Shankland, T.J., 1995. A high P-T single-crystal X-Ray-Diffraction study of thermoelasticity of MgSiO_3 orthoenstatite, *Phys. Chem. Miner.*, **22**(6), 393–398.

APPENDIX A: GLOBAL INVERSION FOR PARAMETER VALUES

Our estimates of the parameters and their uncertainties are given in Table A1. Values of many of the parameters are similar to those given in Ita & Stixrude (1992) except for those phases not included in the earlier study (anorthite, spinel) and for which the values were previously unknown (hpcpx). New to this study are values of G_0 , G'_0 and η_{s0} , and values of q_0 constrained by experimental measurements, as opposed to our previous assumption that $q \approx 1$ for all species. All parameter values are considered better estimates than in our previous work primarily because of the vast expansion in the experimental and first principles theoretical database in the intervening years.

Our strategy for estimating the parameters is based on an iterative global least-squares inversion to a wide variety of experimental data. Cases for which no experimental data exist are discussed further below. We proceed as follows, beginning from initial guesses at the values of all parameters based on our previous studies.

V_0 is set equal to the ambient volume as measured by X-ray diffraction. Properties of fictive end-members (e.g. Fe-wadsleyite, Mg-diopside) are linearly extrapolated from the measured range.

K_0 is set equal to the value of the isentropic bulk modulus as measured by Brillouin or ultrasonic techniques, corrected for the difference between isothermal and isentropic values,

$$K_0 = K_S(P_0, T_0)[1 + \alpha(P_0, T_0)\gamma_0 T_0]^{-1}, \quad (\text{A1})$$

where the correction factor is calculated self-consistently via our thermodynamic model. If Brillouin or ultrasonic measurements of K are not available, we make use of equation of state data. We have not undertaken a re-analysis of room temperature equation of state data. Instead, we set K_0 equal to the value of the isothermal bulk modulus reported in the experimental study.

K'_0 is set equal to the value measured by Brillouin or ultrasonic techniques, corrected for the difference between isothermal and adiabatic values from the isothermal pressure derivative of eq. (A1). When Brillouin or ultrasonic measurements of K'_0 are not available, we make use of equation of state data. In this case, it is important that the values of K_0 and K'_0 are consistent with each other because of the well-known trade-off between these quantities when fitting to equation of state data. If K_0 is taken from a Brillouin or ultrasonic study, we determine the value of K'_0 by fitting to the equation of state data while keeping the value of K_0 fixed at the Brillouin/ultrasonic value (Bass *et al.* 1981). If K_0 is determined from an equation of state study, the value of K'_0 is taken from the same fit from the same experimental study.

θ_0 is determined by requiring that the model reproduce the experimentally determined third law vibrational entropy at 1000 K, or at the highest measured temperature if this is less than 1000 K. We account for the following non-vibrational contributions to the entropy: (i) magnetic, assumed to be $R \ln 5$ per Fe; and (ii) disorder, which we include for spinel and hercynite by assuming an inverse spinel fraction of 25 per cent and ideal entropy of mixing. The entropy is unmeasured for several important phases (e.g. wadsleyite, perovskite). For these, we retain the value from our previous work (Ita & Stixrude 1992; Stixrude & Bukowinski 1993; Stixrude & Lithgow-Bertelloni 2005). We will return in Paper II to the use of phase equilibria data to constrain θ_0 .

γ_0 is determined via a least-squares fit to thermal expansion data, via eq. (21).

q_0 is determined by a least-squares fit to measurements of the bulk modulus at high temperature, via eq. (32), or, if these are not available, to measurements of the pressure–volume–temperature equation of state, via eq. (21).

G_0 and G'_0 are set equal to their values as determined by *in situ* Brillouin or ultrasonic measurements.

η_{s0} is determined by a least-squares fit to measurements of the shear modulus at high temperature via eq. (33).

The global inversion is iterated to self-consistency. Iteration is necessary because some measured quantities are sensitive to more than one parameter: for example, the thermal expansion is influenced by γ_0 and q_0 (Fig. 7), as well as K_0 and K'_0 . We have found that the inversion converges rapidly, typically after three iterations.

We have estimated unknown parameters on the basis of systematics. We assume that K_0 , γ_0 , q_0 , K'_0 and G'_0 are approximately constant across isostructural series so that if constraints exist for one end-member of a phase, but not the others, we assume that the same values apply to all end-members of that phase. In those cases where the entropy is known for only one species of a phase, we estimate the Debye temperature of the other phases by scaling to the elastic Debye temperature. If K'_0 is unknown or poorly constrained, we have assigned $K'_0 = 4$.

The other systematic relationships that we have used are illustrated in Fig. 6. We use the V_S density-systematic

$$V_S \approx a(m) + b\rho \quad (\text{A2})$$

to estimate G_0 for several mantle species particular iron-bearing end-members. We have found a positive correlation between G' and the ratio G/K that we use to estimate G'_0 when necessary. This correlation, based only on mantle species, is consistent with the negative correlation between G' and K/G that has been discussed in previous studies on the basis of a wide range of solids (Duffy & Anderson 1989). We note a motivation for the relationship between G' and G/K that has apparently not been discussed before, via truncation of the finite strain expansion. If we set the coefficient of the third-order term to zero in the shear modulus expansion, we find

$$G'_0 = \frac{7}{3} \frac{G_0}{K_0} + 1, \quad (\text{A3})$$

$$G'_0 = \frac{5}{3} \frac{G_0}{K_0}, \quad (\text{A4})$$

for eqs (22) and (33), respectively. Most experimental data fall in between these two trends. Finally, we have found a significant correlation between dG/dT and G , which we use to estimate values of dG/dT and thus η_{s0} when no measurements of G at high temperature exist.

Table A1. Properties of mantle species.

Phase	Species	Formula	V_0 ($\text{cm}^3 \text{mol}^{-1}$)	K_0 (GPa)	K'_0	θ_0 (K)	γ_0	q	G_0 (GPa)	G'_0	η_{50}	Ref.
Feldspar (plg)	Anorthite	$\text{CaAl}_2\text{Si}_2\text{O}_8$	100.61	84 (5)	4.0 (10)	752 (2)	0.39 (5)	1.0 (10)	40 (3)	1.1 (5)	1.6 (10)	1–5
Spinel (sp)	Spinel	$(\text{Mg}_3\text{Al})(\text{Al}_7\text{Mg})\text{O}_{16}$	159.05	197 (1)	5.7 (2)	900 (3)	1.02 (4)	2.8 (6)	109 (10)	0.4 (5)	2.7 (6)	1,4,6–8
Spinel	Hercynite	$(\text{Fe}_3\text{Al})(\text{Al}_7\text{Fe})\text{O}_{16}$	163.37	209 (2)	5.7 (10)	768 (23)	1.21 (7)	2.8 (10)	85 (13)	0.4 (5)	2.8 (10)	1,2,9,10
Olivine (ol)	Forsterite	Mg_2SiO_4	43.60	128 (2)	4.2 (2)	809 (1)	0.99 (3)	2.1 (2)	82 (2)	1.4 (1)	2.4 (1)	1,8,11–13
Olivine	Fayalite	Fe_2SiO_4	46.29	135 (2)	4.2 (10)	619 (2)	1.06 (7)	3.6 (10)	51 (2)	1.4 (5)	1.1 (6)	1,2,4,5,8,14,15
Wadsleyite (wa)	Mg-wadsleyite	Mg_2SiO_4	40.51	169 (3)	4.3 (2)	881 (100)	1.22 (9)	2.0 (10)	112 (2)	1.4 (2)	2.7 (4)	1,5,16–19
Wadsleyite	Fe-wadsleyite	Fe_2SiO_4	43.21	169 (13)	4.3 (10)	599 (100)	1.22 (30)	2.0 (10)	72 (12)	1.4 (5)	1.1 (10)	16,20
Ringwoodite (ri)	Mg-ringwoodite	Mg_2SiO_4	39.49	183 (2)	4.1 (2)	908 (100)	1.10 (10)	2.8 (4)	120 (2)	1.3 (1)	2.7 (5)	1,5,16,21
Ringwoodite	Fe-ringwoodite	Fe_2SiO_4	42.03	218 (7)	4.1 (10)	685 (100)	1.30 (24)	2.8 (10)	95 (10)	1.3 (5)	1.9 (10)	1,16,21,22
Orthopyroxene (opx)	Enstatite	$\text{Mg}_2\text{Si}_2\text{O}_6$	125.35	107 (2)	7.1 (4)	810 (8)	0.67 (4)	7.8 (11)	77 (1)	1.6 (1)	2.4 (5)	1,2,3–29
Orthopyroxene	Ferrosilite	$\text{Fe}_2\text{Si}_2\text{O}_6$	131.88	101 (4)	7.1 (5)	680 (16)	0.67 (8)	7.8 (10)	52 (5)	1.6 (5)	1.1 (10)	1,2,9,23,30,31
Orthopyroxene	Mg-Tschermak's	$(\text{Mg}_2\text{Al}_2)\text{Si}_2\text{Al}_2\text{O}_{12}$	120.50	107 (10)	7.1 (10)	856 (100)	0.67 (30)	7.8 (10)	68 (10)	1.6 (5)	2.4 (10)	32
Clinopyroxene (cpx)	Diopside	$\text{Ca}_2\text{Mg}_2\text{Si}_4\text{O}_{12}$	132.08	112 (5)	5.2 (18)	782 (5)	0.96 (5)	1.5 (20)	67 (2)	1.4 (5)	1.6 (10)	1,2,5,26,33,34
Clinopyroxene	Hedenbergite	$\text{Ca}_2\text{Fe}_2\text{Si}_4\text{O}_{12}$	135.73	119 (4)	5.2 (10)	702 (4)	0.93 (6)	1.5 (10)	61 (1)	1.2 (5)	1.6 (10)	1,2,5,15,35
Clinopyroxene	Mg-diopside	$\text{Mg}_2\text{Mg}_2\text{Si}_4\text{O}_{12}$	126.00	112 (10)	5.2 (10)	851 (100)	0.96 (30)	1.5 (10)	75 (10)	1.5 (5)	1.7 (10)	36
HP-clinopyroxene (hpcpx)	HP-clinoenstatite	$\text{Mg}_4\text{Si}_4\text{O}_{12}$	121.94	107 (26)	5.3 (40)	768 (100)	0.95 (4)	1.1 (45)	84 (10)	1.8 (5)	1.6 (10)	37
HP-clinopyroxene	HP-clinoferrrosilite	$\text{Fe}_4\text{Si}_4\text{O}_{12}$	128.10	107 (10)	5.3 (10)	617 (100)	0.95 (30)	1.1 (10)	70 (10)	1.5 (5)	1.4 (10)	38
Ca-perovskite (cpv)	Ca-perovskite	CaSiO_3	27.45	236 (4)	3.9 (2)	984 (100)	1.53 (7)	1.6 (16)	165 (12)	2.5 (5)	2.4 (10)	1,39–41
Akimotoite (ak)	Mg-akimotoite	MgSiO_3	26.35	211 (4)	4.5 (5)	850 (100)	1.18 (13)	1.3 (10)	132 (8)	1.6 (5)	2.7 (10)	1,2,5,42
Akimotoite	Fe-akimotoite	FeSiO_3	26.85	211 (10)	4.5 (10)	810 (100)	1.18 (30)	1.3 (10)	158 (10)	1.6 (5)	3.7 (10)	20
Akimotoite	Corundum	Al_2O_3	25.58	253 (5)	4.3 (2)	933 (3)	1.32 (4)	1.3 (2)	163 (2)	1.6 (1)	2.8 (2)	1,4,5,8,43
Garnet (gt,mj)	Pyrope	$\text{Mg}_3\text{Al}_2\text{Si}_3\text{O}_{12}$	113.08	170 (2)	4.1 (3)	823 (4)	1.01 (6)	1.4 (5)	94 (2)	1.3 (2)	1.0 (3)	1,4,44–46
Garnet	Almandine	$\text{Fe}_3\text{Al}_2\text{Si}_3\text{O}_{12}$	115.43	177 (3)	4.1 (3)	742 (5)	1.10 (6)	1.4 (10)	98 (3)	1.3 (5)	2.2 (10)	1,9,45,47,48
Garnet	Grossular	$\text{Ca}_3\text{Al}_2\text{Si}_3\text{O}_{12}$	125.12	167 (1)	5.5 (4)	823 (2)	1.08 (6)	0.4 (4)	108 (1)	1.1 (2)	2.4 (2)	1,4,8,25,45,49,50
Garnet	Mg-majorite	$\text{Mg}_3\text{MgSi}_3\text{O}_{12}$	114.32	165 (3)	4.2 (3)	788 (100)	1.07 (30)	1.4 (5)	85 (2)	1.4 (2)	0.7 (5)	1,46,51
Stishovite (st)	Stishovite	SiO_2	14.02	314 (8)	4.4 (2)	1044 (20)	1.34 (17)	2.4 (22)	220 (12)	1.6 (5)	5.0 (10)	1,4,5,52–54
Perovskite (pv)	Mg-perovskite	MgSiO_3	24.45	251 (3)	4.1 (1)	1070 (100)	1.48 (5)	1.4 (5)	175 (2)	1.7 (2)	2.6 (6)	1,55–58
Perovskite	Fe-perovskite	FeSiO_3	25.48	281 (40)	4.1 (10)	841 (100)	1.48 (30)	1.4 (10)	138 (40)	1.7 (5)	2.1 (10)	20,59
Perovskite	Al-perovskite	AlSiO_3	25.49	228 (10)	4.1 (5)	1021 (100)	1.48 (30)	1.4 (10)	160 (10)	1.7 (5)	3.0 (10)	60,61
Magnesiowüstite (mw)	Periclase	MgO	11.24	161 (3)	3.9 (2)	773 (9)	1.50 (2)	1.5 (2)	130 (3)	2.2 (1)	2.3 (2)	1,4,7,8,44
Magnesiowüstite	Wüstite	FeO	12.06	152 (1)	4.9 (2)	455 (12)	1.28 (11)	1.5 (10)	47 (1)	0.7 (1)	0.8 (10)	1,5,62–64

Italicized entries are from systematics.

References: 1, Smyth & McCormick (1995); 2, Bass (1995); 3, Angel *et al.* (1988); 4, Robie & Hemingway (1995); 5, Fei (1995); 6, Yoneda (1990); 7, Fiquet *et al.* (1999); 8, Anderson & Isaak (1995); 9, Anovitz *et al.* (1993); 10, Harrison *et al.* (1998); 11, Zha *et al.* (1996); 12, Robie *et al.* (1982); 13, Bouhifid *et al.* (1996); 14, Zha *et al.* (1998); 15, Knittle (1995); 16, Sinogeikin *et al.* (1998); 17, Zha *et al.* (1997); 18, Fei *et al.* (1992); 19, Li *et al.* (2001); 20, Jeanloz & Thompson (1983); 21, Sinogeikin *et al.* (2001); 22, Mao *et al.* (1969); 23, Jackson *et al.* (1999); 24, Flesch *et al.* (1998); 25, Thieblot *et al.* (1999); 26, Krupka *et al.* (1985); 27, Jackson *et al.* (2003); 28, Zha *et al.* (1995); 29, Frisillo & Barseh (1972); 30, Hugh-Jones & Angel (1997); 31, Hugh-Jones & Boyd (1964); 32, Skinner & Boyd (1964); 33, Levien & Prewitt (1981); 34, Zha *et al.* (1998); 35, Haselton *et al.* (1987); 36, Tribaudino *et al.* (2001); 37, Shimmei *et al.* (1999); 38, Hugh-Jones *et al.* (1996); 39, Shim *et al.* (2000); 40, Wang *et al.* (1996); 41, Karki & Crain (1998); 42, Dasilva *et al.* (1999); 43, Gieske & Barseh (1968); 44, Sinogeikin & Bass (2000); 45, Thieblot *et al.* (1998); 46, Sinogeikin & Bass (2002b); 47, Sinogeikin *et al.* (1997); 48, Zhang *et al.* (1999); 49, Oneill *et al.* (1989); 50, Conrad *et al.* (1999); 51, Sinogeikin & Bass (2002a); 52, Weidner *et al.* (1982); 53, Andraut *et al.* (2003); 54, Liu *et al.* (1999); 55, Sinogeikin *et al.* (2004); 56, Wentzcovitch *et al.* (2004); 57, Shim & Duffy (2000); 58, Fiquet *et al.* (2000); 59, Kiefer *et al.* (2002); 60, Kubo & Akaogi (2000); 61, Thompson *et al.* (1996); 62, Jackson *et al.* (1990); 63, Jacobsen *et al.* (2002); 64, Stollen *et al.* (1996).

Uncertainties are set to experimental uncertainties, or to the difference between different experimental values if two or more studies of comparable probable accuracy disagree. If the full elastic constant tensor is available, we set uncertainties in G and K to the larger of quoted experimental uncertainties, and the difference between Voigt and Reuss bounds (Watt *et al.* 1976). For those parameters that are determined via least-squares fits to experimental data, the uncertainty is set to the error in the inverted parameter. For parameters that are estimated based on systematics, we have assigned large nominal uncertainties.